Examensarbete
TVVR 14/5011

Evaluation of Global Wave Climate Based on the JMA/MRI-AGCM Climate Change Projection

A Comparative Study of Significant Wave Height Fields for Present and Future Climate, Modelled in the WAM Model

Johanna Ekstedt

Division of Water Resources Engineering
Department of Building and Environmental Technology
Lund University

In collaboration with:
Department of Urban And Environmental Engineering
Kyushu University

Avd för Teknisk Vattenresurslära
TVVR-14/5011
ISSN 1101-9824

Evaluation of Global Wave Climate Based on the JMA/MRI-AGCM Climate Change Projection

A Comparative Study of Significant Wave Height Fields for Present and Future Climate, Modelled in the WAM Model

Johanna Ekstedt

Abstract

In this study global wave climates for present and future climates are simulated with the WAM model, based on wind fields from the JMA/MRI-AGCM3.2 climate projection. The projected wave fields are analysed and compared for the two periods of 1979-2003 and 2075-2099, and climate change induced differences are identified.

It is found that the wave climate is strongly dependent on latitude, with the largest waves, as well as most significant seasonal variations, located at the mid to high latitude regions. These areas are also where the climate induced changes from present to future climate are most noteworthy. The largest increases of significant wave height of approximately +5%, is experienced in the southern parts of the Indian, Pacific and Atlantic Oceans as well as in the Antarctic Ocean. The largest decreases are of the same order, and found to the northern Atlantic Ocean.

In addition, a slightly smaller but widespread decrease is seen in the tropical storm affected region around Japan, in the western Pacific Ocean. In contrast to this reduction of the everyday wave climate, an evaluation of the annual maximum waves at this location indicates that the extreme wave climate might become more severe due to the projected climate change. In the central and lower parts of the mid latitude regions the projected wave climate remain fairly stable and show only minor changes between present and future climates.

It is noted that the processes behind the everyday wave climate differ significantly from those causing extreme events, and that the phenomena should therefore be evaluated separately. Since this study focuses on the climate change induced effects on the wave climate under normal weather conditions, it is recommended that in future research evaluate the extremes in a more thorough manner. For that analysis using the full potential of the JMA/MRI-AGCM high-resolution wind fields output is recommended.

Contents

1 Introduction

Waves and the general conditions of the oceans affect coastal regions and marine activities on a daily basis, all over the world. It is becoming increasingly clear that human activity is affecting not only the atmospheric climate, but also the characteristics of our oceans. As the composition of the atmosphere changes and the concentration of green-house gases increases the impact on the environment as a whole steadily grows.

The ocean climate is affected by increasing temperatures in many different ways. A static side-effect of global warming is for example the thermal expansion of the oceans resulting in rising sea levels. Effects of this phenomenon can already be seen in many coastal regions where coastal erosion and inundations are common problems. According to the IPCC (2007) the sea-level has risen by 1.7 ± 0.3 mm/year since the second half of the 19th century and the rate seems to have increased during the last decade.

The dynamic side-effects of the warming climate are the expected changes of the behaviour of ocean waves, storm surges and other extreme events (IPCC, 2007). Reports of increased extreme climate in many parts of the world make the importance of understanding and assessing the effects of climate change greater than ever before. The number of coastal and marine activities and applications which are dependent on reliable and long-term information about wind and wave climate are also constantly increasing, and with that the necessity of predictions and forecasts of future development.

Many contemporary studies within the field of wave climate prediction are focused on extreme events such as tropical storms and wave fields during extreme weather. In this study, however, the main focus will be on average wave climate and wave evolution under normal conditions. The aim is to evaluate the effects of climate change and compare wave climates for the projected present and future periods.

The analysis is conducted on a global scale but also, a few locations are chosen for a more thorough analysis of regional wave climate in different parts of the world. This regional analysis also includes a basic evaluation of extreme wave conditions, including the estimation and comparison of return values for the 50 and 100 year return periods. The wave predictions which are analysed are modelled by the WAM numerical wave model with input wind fields from the JMA/MRI-AGCM3.2. This is an Atmospheric General Circulation Model of which the second version was recently developed through the collaboration between the *Japanese Meteorological Agency*, JMA, and the *Meteorological Research Institute*, MRI.

2 Background

This first chapter is intended give some useful background information that is important for the understanding of the study at hand. Initially, in section 2.1, a basic introduction to ocean waves is given, presenting notions and relationships that make up the foundation of the characteristics and evolution of a wave field. The understanding of basic wave theory is also essential for the concept of numerical modelling of waves.

In section 2.2 the basic ideas connected to climate change projection are introduced, together with an explanation concerning the concept of greenhouse gas emission scenarios. In addition, the climate projection model utilized to simulate the wind fields in this study, the JMA/MRI-AGCM3.2, is described and a brief summary of previous research related to the theme of this study is presented.

In the last subsection, section 2.3, the processes and underlying mathematical parameterizations of numerical modelling of ocean waves, are explained and the basic ideas behind the WAM model is introduced.

2.1 Introduction to Ocean Waves

Ocean surface waves are created by natural forces such as wind-generated pressure and stress, earthquakes, gravitational forces from the Earth, the sun and the moon, as well as the surface tension of water (WMO, 1998). Consequently, owing to the diversity of these energy input sources, the sea-state is usually made up by a complex combination of waves ranging from large-scale movements, such as tidal waves, to very small-scale, capillary waves. In this report the main focus will be on mid-range waves, generated by winds and Earth's gravitational force.

Wind-generated gravity waves are, as the name implies, waves which are generated by a wind field somewhere on the ocean. Whilst under the direct influence of winds, these waves are highly irregular and are commonly referred to as *wind-sea*. When travelling out and away from the fetch in which they were generated however, the waves turn into *swell*, which are more regular, long-crested waves and which can travel thousands of kilometres across the ocean. Since wind-generated waves are almost constantly present at sea, they constitute an important factor for activities such as shipping, fishing, off-shore industries as well as for the processes involved in coastal erosion and sediment transport. In addition, the global climate is greatly affected by ocean-atmosphere interactions such as the exchange of heat, energy and gases (WMO, 1998).

When attempting to describe the complex world around us, the development of simplified models is usually essential. For ocean waves, the crudest description is based on *linear wave theory*, depicting wave movements as simple sinusoidal,

long-crested, progressive waves. For this theory to be valid the following assumptions are made (WMO, 1998):

- The density of water is constant (water is incompressible) which makes it possible to derive a continuity equation for the fluid.
- The only forces acting on a water-particle is gravity and pressure (thus friction is ignored).
- Individual water particles do not rotate but can only move around each other.

The basic characteristics of a linear wave are shown in figure 2.1, where the displacement of the sea surface, η, from mean sea-level is illustrated by a sinusoidal wave:

$$\eta(x,t) = a\sin(kx - \omega t)$$

with amplitude, *a;* wavenumber, $k = 2\pi/\lambda$*;* wavelength, λ*;* angular frequency, $\omega = 2\pi/T$ and period, *T*. The wave height, *H*, is defined as the vertical distance between the crest and the through of a wave, thus *H=2a.*

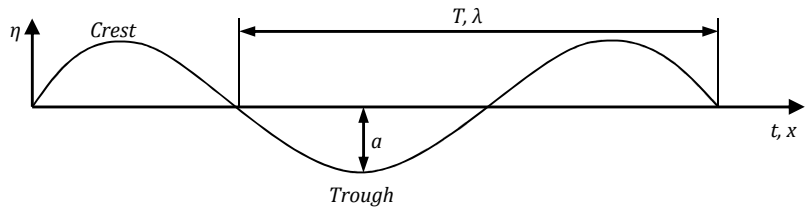

Figure 2.1 - Parameters describing a linear harmonic wave, with surface elevation, η: period, T, wavelength, λ and amplitude a.

In reality, this kind of regular wave does not exist at sea, even though the appearance of swell can sometimes come reasonably close. In the analysis of records of real waves the first step usually consists in the identification of individual waves. This is not as straightforward as in the case of the harmonic waves described above, since a record of surface elevation is irregular by nature and a wave thus can include more than one local maximum or minimum point.
A common approach to define the limits of individual waves is by the up-crossing (or down-crossing) method. Applying this method means that a wave is recognised as the surface elevation profile in between two subsequent crossings of a predefined reference zero-level (Holthuijsen, 2007). The wave height is then

identified as the vertical distance between the maximum and minimum surface elevation within such a profile, and the wave period is the time between the two crossings of the reference level.

Wave fields at sea are generally highly irregular, with waves constantly overtaking and crossing each other. Because of this unpredictability and randomness of ocean waves they are best described based on probabilistic theory (Reeve, 2011). Statistical methods of analysis will be discussed further in section 3.3.

To illustrate a tree-dimensional and random sea-state, a much more complex representation is needed than solely the harmonic waves described above. However, harmonic waves and linear theory can act as a foundation for more complex models. The three-dimensional description of ocean wave fields can be made in terms of harmonic waves moving through an x-y-space, which, mathematically can be written as (Holthuijsen, 2007):

$$\eta(x, y, t) = a\cos(\omega t - kx\cos\theta - ky\sin\theta + \alpha)$$

where a is the amplitude, k is the wave number, ω , is the angular frequency, θ is the direction of wave propagation, normal to the wave crest, and α is the phase of the wave.

In order to further represent a random sea-state, the three-dimensional random-phase/amplitude model is used, describing the super-positioning of a large number of the propagating harmonic waves, described above (WMO, 1998; Holthuijsen, 2007). This idea is visually illustrated in figure 2.2 below.

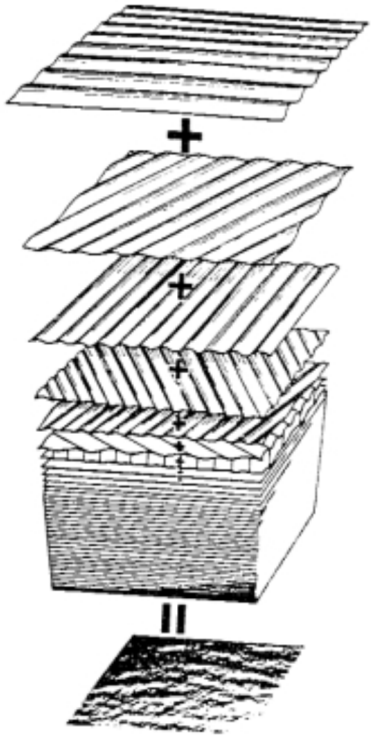

Figure 2.2 – Super-positioning of several harmonic waves of different amplitude, direction and phase can realistically illustrate the random nature of a natural sea state (Pierson, Neumann, & James, 1955).

The result of this model determines the basic concept for the notion of the *wave spectrum* and the super-positioning of waves can mathematically be described as:

$$\eta(x,y,t) = \sum_{i=1}^{N}\sum_{j=1}^{M} \underline{a}_{ij} \cos\left(\omega_i t - k_i x \cos\theta_j - k_i y \sin\theta_j + \underline{\alpha}_{ij}\right)$$

When waves move across a sea-surface they usually group together and form a *wave group* containing waves of similar wavelengths. Individual waves within the group, move at a speed, c, which is related to their wavelength, λ, through: $c = \lambda/T$, where T is the period (WMO, 1998). However the wave group as a whole, move at a different speed called *group speed,* which for deep water is approximately equal to:

$$c_g = \frac{c}{2}$$

When a wave group crosses the ocean the water particles it passes move in near circular motions (in shallow water, however, the path is closer to elliptical), making the horizontal movement of the water very limited. The wave motion is in fact an oscillating transformation between kinetic and potential energy, the former disturbing the water and the latter vertically displacing water particles between the crest and through of the passing wave (WMO, 1998). The energy contained in a wave is continuously altered through advection which can be expressed through the energy balance for ocean waves (Janssen P. , 2004):

$$\frac{\delta F}{\delta t} + \nabla \cdot \left(c_g F\right) = S = S_{in} + S_{ds} + S_{nl}$$

This equation describes the development of the surface gravity wave field in time and space and is based on the two-dimensional wave spectrum F(f,θ,x,t) with frequency, f, direction of propagation, θ and the group velocity, c_g. The source terms on the right-hand side of the equation make up the total energy, *S*, which is the sum of external gains, S_{in},; dissipative losses, S_{ds}, and the non-linear wave-wave interactions, S_{nl} (WMO, 1998). The wave energy source terms establish the basis for many numerical wave models, which is further discussed in section 2.3.

2.2 Climate Change Projection

In the Fourth Assessment Report of the *Intergovernmental Panel on Climate Change,* IPCC, it is concluded that the climate change development, experienced since the middle of the last century, would have been very unlikely to occur based exclusively on natural sources of climate variability (IPCC, 2007). It is also stated that the external forces at work are very likely to be caused by the change of greenhouse concentration in the atmosphere. However, the experienced warming of the climate is thought to have become much greater, were it not for the cooling effect related to the simultaneous increasing concentration of atmospheric aerosol and similar substances.

It is already well known that human activity is, to a great extent the cause for recent warming of the global climate. In connection to the atmospheric temperature alterations, the world oceans are also affected by this anthropogenic climate forcing, and according to the IPCC (2007) the top few 100 meters of the oceans have experienced warming during the latter part of the 20th century.

Due, mainly to the thermal expansion of water, many parts of the world have lately experienced accelerating sea-level rise as a result of the changing climate. Studies show that the average yearly rise of the sea-level was 1.7 mm ± 0.3mm in between 1870 to 2004 but that the rate has increased during the last decade (Mori, Yasuda, Mase, Tom, & Oku, 2010). Sea-level rise in itself can cause many problems,

especially to coastal areas which both are threatened by inundation and are made more vulnerable to other processes such as the effects of severe storms and high waves. While sea-level rise is a static side effect of climate change, the dynamic part, such as ocean waves and storm surges, are also expected to change with the warming climate. According to the IPCC (2007) it is more likely than not that anthropogenic influence have played a part in the increasing frequency of intense tropical storms in many parts of the world.

Clearly, climate change results form a complex mix of different influences and processes. Nonetheless, as the change protrudes and to a larger extent affects various activities on earth, the need and interest in describing and predicting future climate change continue to grow. In order to project plausible development scenarios several types of climate models are today used to simulate future climate. These models translate changes in e.g. the atmospheric composition of gases into a climate response based on numerous physical processes which are mathematically represented in the models (IPCC, 2001). The basic steps of a climate projection process can be summarized as:

- a projection of future changes of emissions
- resulting changes in atmospheric greenhouse gas and aerosol concentration
- a model describing these changes

In studies of future climate change a hierarchy of different coupled models describing the ocean, atmosphere, sea-ice and land-surface interactions are often used. The input to the models varies depending on the characteristics that are of interest. A common procedure is to run a model with a yearly increase of atmospheric CO_2 of 1% until the initial concentration is doubled and then keeping the rate steady. Increases of this magnitude of CO_2 alone has yet not been measured, however, the CO_2-concentration in these models is thought of as the *equivalent* CO_2 concentration of the total radiate effect from all green-house gases in the atmosphere, making a 1% yearly increase a plausible estimate. Another common approach, utilized in climate projection is to follow a prescribed emission scenario. In this study one of the IPCC scenarios is used as basis for the climate projection. This specific scenario, as well as the notion of emission scenarios in general is more closely described in the next subsection.

For this study the MRI/JMA- Atmospheric General Circulation Model (AGCM) is used in the climate projection. An AGCM, also called a mixed-layer model, typically contains equations that describe the evolution of temperature, wind, precipitation, pressure and water vapour processes which, in turn are coupled to a non-dynamic model corresponding to the upper ocean. In contrast to more detailed climate

models, such as Atmospheric-Ocean General Coupled Models (AOGCM), the atmosphere-sea interaction in an AGCM is limited to the response caused by sea surface temperatures (SST), i.e. no dynamic responses are simulated (IPCC, 2001). Even though the AGCM, for this reason, cannot portray atmosphere-ocean interactions as completely as an AOGCM, which includes effects from the full ocean depth, the advantage of reduced computing requirements make it possible to conduct global-scale computations with higher spatial resolution and for longer periods of time (Mizuta, et al., 2011; IPCC, 2001).

Climate change is, as has already been touched upon, a combination of natural variability and forced variability. In climate change projections both components are simulated (IPCC, 2001), however, it is the forced climate change, such as changes in atmospheric greenhouse gas concentration provoked by human activities, which is of interest in the future climate predictions. Since the influence of the natural variability, also called climate noise, can obscure results, measures are commonly taken to reduce its impact. This natural climate variability is a random phenomenon and can therefore often be averaged out over an ensemble of model runs with no, or constant forcing. The overall forcing can be expressed in terms of the heat balance:

$$\frac{dH}{dt} = F - \alpha T$$

where dH/dt is the rate of heat storage, F is the radiative forcing change and αT, represents the combined effects counteracting increased heat storage.

Naturally there are many uncertainties involved in the process of climate change projections. Initially, it is impossible to foretell how the future will unfold, making the uncertainty connected to forcing scenarios imminent. Since it is unrealistic to expect one single scenario to correctly depict the future, models are often run for several different scenarios to give a range of possible future climate change responses (IPCC, 2007).

Another uncertainty factor lies within the models and the modelled response to an input emission scenario. There is always a risk that some physical processes are missed, or misinterpreted. To evaluate model performance several different models can be run with the same forcing. The differences between the results can then be evaluated to give an idea about the accuracy and precision of model responses.

2.2.1 Climate Change Scenarios

In 1990 and 1992 the Intergovernmental Panel on Climate Change put forward a number of long-term emission scenarios, concerning greenhouse gases (GHG) and sulfur emissions in order to facilitate the analysis of possible future climate change. In 1996, at the time of the publishing of the IPCC Third Assessment Report's (IPCC, 2001), the scenarios were revised, based on new knowledge, and were presented in the Special Report on Emission Scenarios (IPCC, 2000).

The SRES scenarios are divided in to four different *families*, A1, A2, B1 and B2, each founded on a narrative storyline, describing future emissions based on a number of driving forces. The storylines describe demographic, economic, social, technological and policy-regulated factors that all have impact on the rate an extent of future emissions. Within each family the basic narrative has in turn been interpreted and quantified in different ways and by different models, creating a total of 40 SRES scenarios. Together the scenarios describe a range of possible futures, and IPCC underlines that no one scenario is more likely or probable than any other.

The scenario used in the MRI/JMA-AGCM3.2 projection, and thus the scenario which is at the core of this study is the so-called marker scenario of the A1 family, A1B. This scenario and its narrative background will be described below, whereas further information on the remaining scenarios can be found in the IPCC Special Report on Emission Scenarios. In that report the storyline behind the A1 family is summarized as follows (IPCC, 2000) :

> *The A1 storyline and scenario family describes a future world of very rapid economic growth, global population that peaks in mid-century and declines thereafter, and the rapid introduction of new and more efficient technologies. Major underlying themes are convergence among regions, capacity building, and increased cultural and social interactions, with a substantial reduction in regional differences in per capita income. The A1 scenario family develops into three groups that describe alternative directions of technological change in the energy system. The three A1 groups are distinguished by their technological emphasis: fossil intensive (A1FI), non-fossil energy sources (A1T), or a balance across all sources (A1B).*

The A1B scenario was chosen as the marker scenario for the A1 family, not because it is more probable than the others, but because it was thought to best describe the underlying A1 narrative. In this context the *balanced* is meant to indicate that no energy source is put over any other, on the assumption that similar improvement rates would be achieved for all energy supply technologies (IPCC, 2000)

2.2.2 JMA/MRI AGCM

In this study, projected future wind fields from the JMA/MRI-AGCM3.2 is used as input to the WAM model, in order to simulate wave fields for the periods 1979-2003 and 2075-2099. The AGCM3.2 is the most recent version of a model created by the Meteorological Research Institute (MRI) in collaboration with the Japanese Metrological Agency (JMA) intended for climate simulations as well as weather predictions (Mizuta, et al., 2006). The model can, for example, give information on possible future changes of tropical cyclones, the East Asian Monsoon, extreme events and other changes induced by global warming (Mizuta, et al., 2011; Mori, Yasuda, Mase, Tom, & Oku, 2010).

When the initial version, JMA/MRI-AGCM3.1, was developed it was the first climate model that could stand long-time integration while being able to conserve mass and simulate realistic high-resolution global climate. The model can simulate global climate with a horizontal grid size as fine as around 20 km, a grid size corresponding to that which is usually only employed for *Regional Circulation Models* (RCMs) (Mizuta, et al., 2011). One advantage with a high-resolution global model, over RCMs with similar resolution, is that problems with lateral boundary conditions can be avoided. Also the AGCM provides information on regions that have not been covered by a RCM simulation (Mizuta, et al., 2006).

The initial model version, 3.1, was constructed from the JMA operational numerical weather prediction model. In the second version, 3.2, only smaller changes, including new parameterization schemes, were made in order to increase the accuracy of the model performance (Mizuta, et al., 2011). To project future climate, ensemble means of sea surface temperatures (SST) and related oceanic conditions from different atmosphere-ocean coupled GCM runs from the *Coupled Model Inter-comparison Project phase 3* (CMIP3) is used as forcing in the model (Mori, Yasuda, Mase, Tom, & Oku, 2010; Suzuki, Sato, & Michihiro, 2011). Since the results from the CMIP3 originate in multi-model ensemble experiments, uncertainties connected to model errors are reduced. For the present climate, observed SSTs are used as input forcing boundary conditions (Mori, Yasuda, Mase, Tom, & Oku, 2010).

The validity of the two model versions has been experimentally evaluated and compared to observed, and reanalysis climatologies by researchers of the MRI and JMA. These experiments will only be briefly touched upon here but a more thorough account, as well as a complete description of the model parameterizations, can be found in the two articles by Mizuta et al. from 2006 (model version 3.1) and 2011 (model version 3.2).

In Mizuta et al. (2011) a present-day climate experiment was performed with the JMA/MRI-AGCM3.2, based on observed SST. The results were compared to corresponding output from the same experiment performed with the prior model

version (Mizuta, et al., 2006) as well as to observed and reanalysis climatologies. The results of the experiments showed that the AGCM, especially version 3.2, can simulate the global climate in a realistic manner.

In figure 2.3 below, seasonal averages of zonal wind velocities for the two model versions are shown and compared to the Japanese 25-year Re-Analysis (for more information on the JRA25, see Onogi et al (2007)). The diagrams show that the zonal winds correspondence to the JRA25 is improved in version 3.2 compared to version 3.1, with especially good results in the extra-tropics of the Southern Hemisphere for the period December to February (Mizuta, et al., 2011).

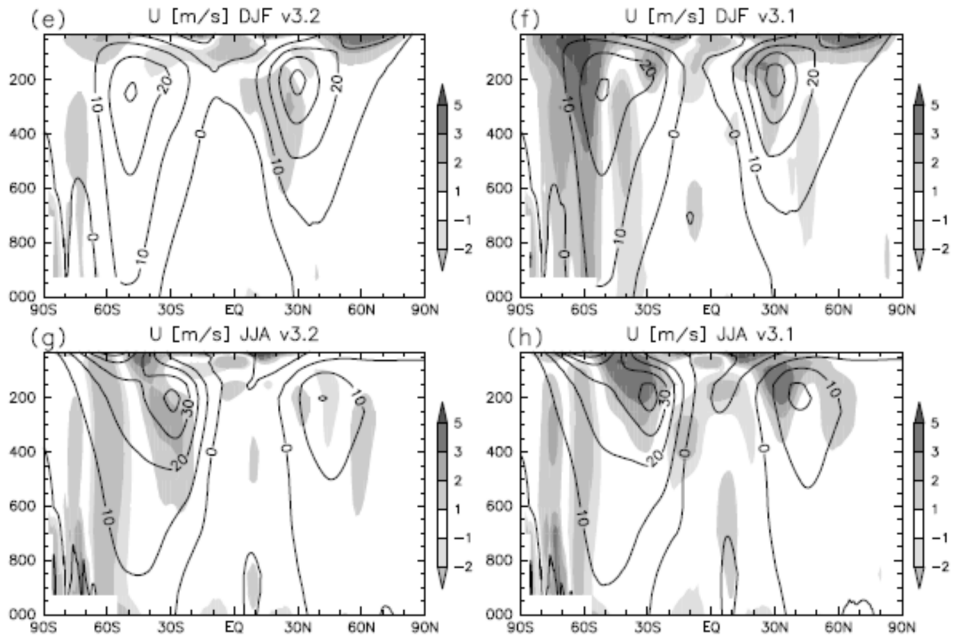

Figure 2.3 - Seasonal averages of zonal wind velocities (m/s) with shading representing differences from the JRA25 reanalysis. DJF=December-January-February and JJA=June-July-August (Mizuta, et al., 2011).

In addition, a skill-score test (initially defined by Taylor (2001)) was performed for the two models, comparing observed and model-simulated monthly-mean spatial samples of various variables. When comparing the models' standard deviations and correlation coefficients to those of an observed climatology most variables were found to be better in the AGCM3.2. Also, it was shown in the experiments of Mizuta et al. (2006) that the accuracy of the results produced by the AGCM3.1 was dependent on the resolution of the model grid, with higher resolution resulting in higher accuracy. However, this dependence was shown to be small in the case of the AGCM3.2 which is a welcome improvement for the work documented in this

report since it relies on wind fields calculated with a grid size of 1 degree, hence a lower resolution than in the experiments presented above.

2.2.3 Related research

There have been numerous studies performed, assessing effects of future climate change, both for the static effects such as sea level rise, as well as on the dynamic side-effects, in which the change of wave climates is included. A large part of these studies are, understandably focused on the development of future extreme events such as tropical storms and cyclones. Very few studies have, however been done on the global scale effects of climate change on ocean waves.

One study that does consider global effects is presented in Mori et al. (2010). In this report a similar study to the one presented here is described, using the wind fields simulated by the MRI/JMA-AGCM3.1 to model the past, close future and future average and extreme wave in the SWAN model. When comparing averaged values of the significant wave height over the periods, 1979-2003, 2015-2031 and 2075-2099, Mori et al. (2010) find that the changes in wave climate over time have a strong latitude dependency. According to the results presented, the mean wave heights will increase both in mid-latitudes areas, as well as in the Antarctic Ocean, whilst the equatorial region as well as the area off the coast of Japan will experience decreased average wave heights. However, this latter area, in the proximity of the Japanese islands, is projected to experience increased magnitudes of extreme waves due to tropical cyclones.

Finally, Mori et al. (2010) underlines that global scale pressure change, causing the average wave climate changes, have a different impact on the wave climate than does the alteration of tropical cyclones. The two phenomena should therefore be studied separately in future research.

Another study concerning the future development of significant wave height is described in Wang et al. (2004), where a statistical model was applied to the output from the CGCM2 (Canadian Centre for Climate Modelling and Analysis) coupled atmosphere-ocean model for three different emission scenarios. The analysis was limited to the future wave fields of the North Atlantic Ocean. It is found that the monthly wave height in the north-east Atlantic Ocean as well as in the south-western North Atlantic will increase towards the end of the 21st century while decreases were projected for the mid-latitudes.

As mentioned, many studies assessing the future of tropical cyclones and other extreme events have been made. The study presented in this report does not include an analysis concerning the development of this kind of events since the resolutions of the model used is considered too low to give a satisfactory result. However, since the impact of tropical and extra-tropical cyclones is dominating

large regions of the world and a short review of some previous studies is presented below.

According to the IPCC (2007), it is likely that all tropical ocean basins have warmed due to influence from human activities throughout the course of the last century, and that it is more likely than not that anthropogenic influence have also played a part in the increasing frequency of intense tropical storms in many parts of the world. As the global warming continues it seems plausible that the conditions for development of tropical storms, also in the future will be favourable, thus increasing their frequency.

On the other hand, there are studies that predict a decreasing frequency and magnitude of tropical cyclones, for example due to increasing vertical wind shear in many parts of the world. According to Weisse and von Storch (2009) tropical cyclones might vary in many different ways due to greenhouse gas induced warming, e.g. changes of frequency, intensity, size, duration or track. This complexity makes the future development hard to predict, especially with large-scale models.

In Murakami et al. (2011), a 60-km resolution version of the JMA/MRI-AGCM3.1 is employed to simulate tropical cyclones for the period 2075-2099. The model show consistent reduction of tropical cyclones, both in genesis numbers and in frequency in the western North Pacific, South Indian Ocean and South Pacific. However the model run shows increases in the central Pacific. In this study as well, the large uncertainty related to simulations of tropical cyclones is mentioned.

Finally, Kitoh et al (2009), use the JMA/MRI-AGCM model to assess future weather extremes based on the evolution of tropical cyclones. The model is used with a grid size as fine as 20-km, making the simulation of tropical cyclone characteristics more accurate than for larger-scale models. The projections show more frequent future occurrence of weather extremes, such as heavy rains.

2.3 Numerical Modelling

Numerical modelling of ocean waves is needed in order to describe and predict the behaviour of ocean waves, when observations of wave characteristics are unavailable. The only way to get around the need for direct measurements of waves is then to simulate wave conditions based on wind data (Holthuijsen, 2007).

A wind field is, in reality a complex system consisting of random movements in three spatial directions and over time. In wave modelling, however, the wind field is simplified into a single horizontal component at each grid point, based on an average values for a specified time-interval. Naturally, the quality of the wind input is of great importance for the final outcome of the wave simulations, even more so since the effects of errors are cumulative in the wave simulation process (WMO, 1998).

Numerical wave prediction models have been operational since the 1960. However, as both knowledge and computer power has grown, the previous models, i.e. first and second generation models, left something to be desired in terms of accuracy and spatial resolution. The most significant improvement from earlier model versions to the current third-generation models is that they solve the basic transport equation and calculates a two-dimensional wave spectrum without the need for prior assumptions about the spectral shape (Janssen P. , 2004). The model used to simulate the wave fields analysed in this report is such a third generation model. It is simply known as the *WAve Model*, WAM, and is described in the following section.

2.3.1 WAM

The numerical model used for this study, is thus, a third-generation wave prediction system called the WAM model, originally developed by the Europe-based *Wave Model Development and Implementation* group (WAMDI). One of the main purposes of the model was to enable operational wave prediction on a global scale (Janssen P. , 2004). The first global version of the model was ready for use in 1992, and has since then been implemented at numerous institutions all over the world. Naturally, the WAM model has been revised over the years, adding improved numerical schemes for e.g. advection, time-integration and interpolation of wave stress. However, the physical source functions remain the same as in the initial version (Janssen P. , 2004).

As mentioned above the great improvement in the third-generation wave models, compared to prior versions, is that no initial and limiting assumptions about the shape of the wave spectrum is required. The shape of the wave frequency spectrum depends on e.g. white capping and wind input and also on the non-linear, internal transfer of energy from the high-frequency end of the spectrum to the lower regions (WAMDI Group, 1988).

In first- and second-generation wave models, this non-linear source term was either completely left out, or initial assumptions forcing the spectrum towards a certain shape were required. These limitations affected the reliability of the model's performance, especially when confronted with complex wind seas and extreme events. In addition, difficulties could often emerge during the transformation of wind sea into swell (WAMDI Group, 1988). In contrast, the WAM model leaves the spectrum free to take on any shape, making the description of the ocean surface more accurate as well as universally valid.

As has already been mentioned, the core of the WAM model lies in the evolution of the two-dimensional ocean wave spectrum, $F(f, \theta, \phi, \lambda, t)$ with respect to frequency and direction of propagation, θ as a function of latitude, ϕ and longitude, λ. The net source function, S, of the energy balance introduced in

section 2.1, can also be described terms of the frequency spectrum through the *transport* or *action balance equation* (WAMDI Group, 1988; ECMWF, 2011):

$$\frac{\delta F}{\delta t} + (\cos\phi)^{-1}\frac{\delta}{\delta\phi}\left(\dot{\phi}\cos\phi\, F\right) + \frac{\delta}{\delta\lambda}\left(\dot{\lambda}F\right) + \frac{\delta}{\delta\theta}\left(\dot{\theta}F\right) = S$$

The parameters $\dot{\phi}, \dot{\lambda}$ and $\dot{\theta}$, refer to the rates of change, for a wave group, of position and direction, respectively here expressed as in the WAMDI (1988):

- $latitude$: $\dot{\phi} = \frac{d\phi}{dt} = c_g R^{-1}\cos\theta$
- $longitude$: $\dot{\lambda} = \frac{d\lambda}{dt} = c_g \sin\theta\,(R\cos\phi)^{-1}$
- $direction$: $\dot{\theta} = \frac{d\theta}{dt} = c_g \sin\theta\tan\phi\, R^{-1}$

with group velocity, $c_g = g/4\pi f$ and *R,* corresponding to the radius of the Earth.
The source terms of the WAM model for the deep water mode, S_{in}, S_{nl} and S_{ds} are super-positioned to represent wind input, non-linear transfer and dissipation due to white-capping:

$$S = S_{in} + S_{ds} + S_{nl}$$

The S_{in}-source term is as mentioned earlier, the representation in the model of the energy input from the wind-wave interactions. This is the only energy input source and the transfer to the waves is effected by the drag force exerted on the surface by the wind. The loss off energy thorough dissipation and white-capping or breaking waves is represented in the WAM model by the S_{ds}, source term. The nonlinear redistribution of energy within the wave spectrum is caused by wave-wave interactions and is described by the, S_{nl}, source term. Basically, energy is moved from higher frequencies towards lower, thus causing a reduction of the peak frequency and a narrowing of the spectrum with time (ECMWF, 2011).
For the case of finite depth, known as shallow water mode in the WAM model, an additional source term, S_{bf}, for bottom friction is included in the energy balance, and the remaining terms are adapted to the dependence on water depth (WAMDI Group, 1988). In this study the WAM is run in so called *deep water mode* and consequently, bottom fiction is disregarded. For a more thorough record of the variables and functions making up the WAM model including shallow water adaptation, see for example the WAMDI Group's original publication: *The WAM Model – A Third Generation Ocean Wave Prediction Model* from 1988. The

numerical modelling condition employed for the current study is presented in section 3.2.

3 Methodology and data

The study presented in this report can be divided into a few individual steps. The analysis is based on two time-slice experiments conducted for the two climate periods

- Present climate: *January 1979 – December 2003*
- Future climate: *January 2075 – December 2099*

The climate model used is the MRI/JMA-AGCM3.2 which has already been introduced in section 2.2.2. The external forcing data is sea surface temperature (SST) which is used as bottom boundary condition for the climate model simulations. For the present day climate, observed SST is used, and for the future climate the SST, projected in multi-model atmosphere-ocean GCM runs from the CMIP3. The conditions for the climate projection and green-house emission levels are based on the SRES A1B scenario introduced in section 2.2.1.

The second part of the study concerns the numerical modelling in WAM, of the wave climates for the two concerned periods. The wind fields projected by the AGCM, containing winds 10 meters above the sea surface, U_{10}, are used as input to the numerical wave model. The model output such as significant wave heights, H_s, are stored for every hour.

To give an idea of how realistic the modelled wave climate is, simulated values for significant wave height as well as for wind speed are compared to observed values from the *American National Oceanic and Atmospheric Administration's* (NOAA) *National Data Buoy Center*. This validation procedure is described in section 3.1.

Finally, the long term wave climate characteristics are statistically analysed and compared between present and future climate simulations. The analysis focuses mainly on the differences in everyday wave conditions between the past and the future wave climate simulations, both on a global scale and at a few chosen locations. The statistical methods and theories that are implemented during the analysis are presented in section 3.3, below. The final results are presented and discussed in section 4.

3.1 Evaluation of Model Performance

In order to gain knowledge about the correspondence between observed values of wind speed and wave height and the simulated wave climate from the WAM

model and the wind fields simulated by the AGCM, a comparative validation is performed. The input wind fields provide one of the most fundamental elements for numerical wave modelling since they are the only source of energy input to the system. This relation consequently makes the importance of accurate wind information much greater since erroneous wind fields result in even larger errors in the wave simulations.
For the validation process the modelled wind and wave records at three locations in the northern Pacific Ocean are compared to observed records measured by three NOAA buoys. The three buoys used for the comparison are: a NOMAD buoy in the Gulf of Alaska known as station 46001 and two discus buoys, stations 51002 and 51003, placed south of Hawaii. Some buoy characteristics are presented in table 3.1.

Table 3.1 – Locations and local wave depth for NOAA buoys 46001, 51002 and 51003 and the location of the model grid points to which the buoy observations are compared.

Station	*Location*		*Water depth*	*Period of available data [yrs]*	*Compared to modelled values from:*	
	Latitude	*Longitude*			*Latitude*	*Longitude*
46001	56.300°N	148.021°W	4206 m	25 yrs (1979-2003)	56°N	148°W
51002	17.094°N	157.808°W	5002 m	20 yrs (1984-2003)	17°N	158°W
51003	19.018°N	160.582°W	4919 m	20 yrs (1984-2003)	19°N	161°W

These buoys are chosen since they have wave records containing both significant wave height and wind speed measurements covering most of the simulated present climate period, 1979-2003. Buoy 46001 has a data for the whole period while the buoys outside Hawaii have records dating back to 1984, thereby enabling 20 years comparison.
It is worth noting the limitations of a validation process such as the one performed in this section. Due to the fairly low resolution of the model used in this study, modelled values chosen for comparison, does not in fact come from the exact same location as the observes counterparts. Also there might be complications connected to the fact that the buoy observation represent point measurements, while the modelled values are only defined for a grid of one degree resolution. Taking this into account, the following evaluation is still believed to be able to give an indication of the overall agreement of modelled and observed values.

The wind and wave projections are evaluated by comparing the distributions of hourly values of wind speed and significant wave height at the tree locations, illustrated in figure 3.1 (46001), figure 3.2 (51002) and figure 3.3 (51003). In addition, the mean value of the distributions are compared for modelled and observed values, as well as the spread of the distribution, based on the range between the 10^{th} and 90^{th} percentile (for information about statistical parameters see section 3.3).

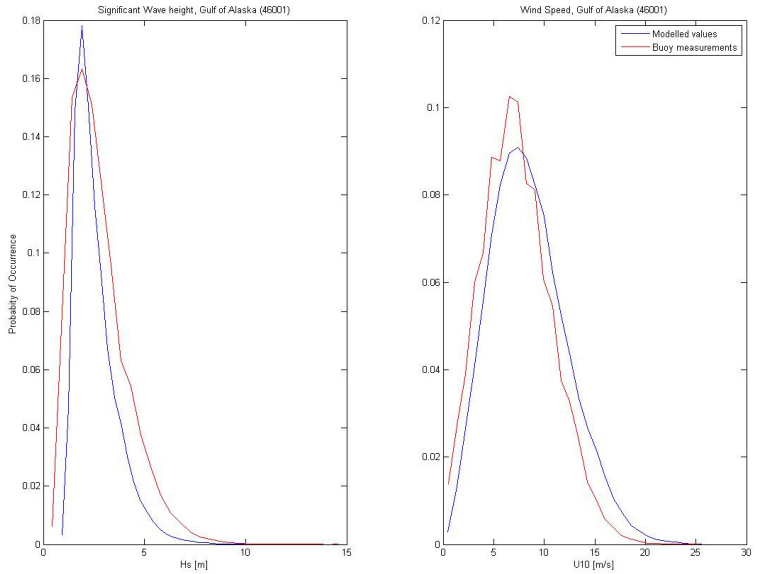

Figure 3.1- Probability density plots for significant wave height, H_s, and wind speed at 10 m height, U_{10}, for modelled values and observations from NOAA buoy station 46001 located in the Gulf of Alaska. The comparison is based on hourly data for the period 1979-2003.

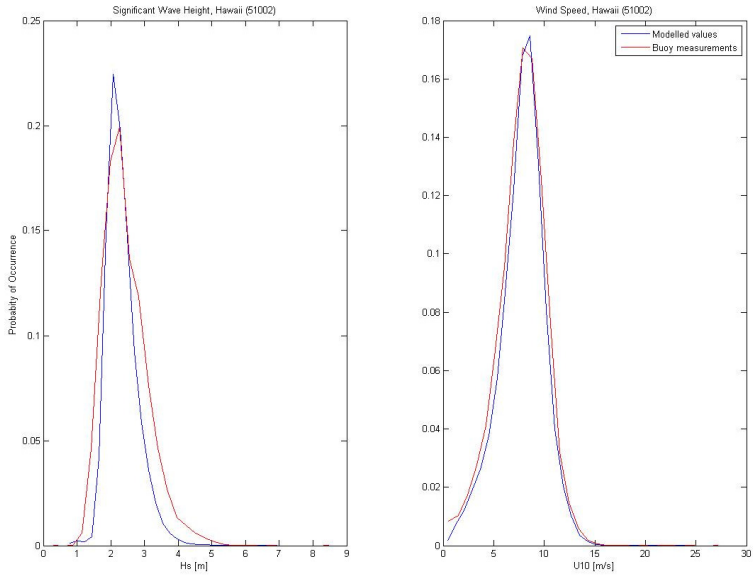

Figure 3.2 - Probability density plots for significant wave height, H_s, and wind speed at 10 m height, U_{10}, for modelled values and observations from NOAA buoy station 51002 located South of Hawaii in the Pacific Ocean. The comparison is based on hourly data for the period 1984-2003.

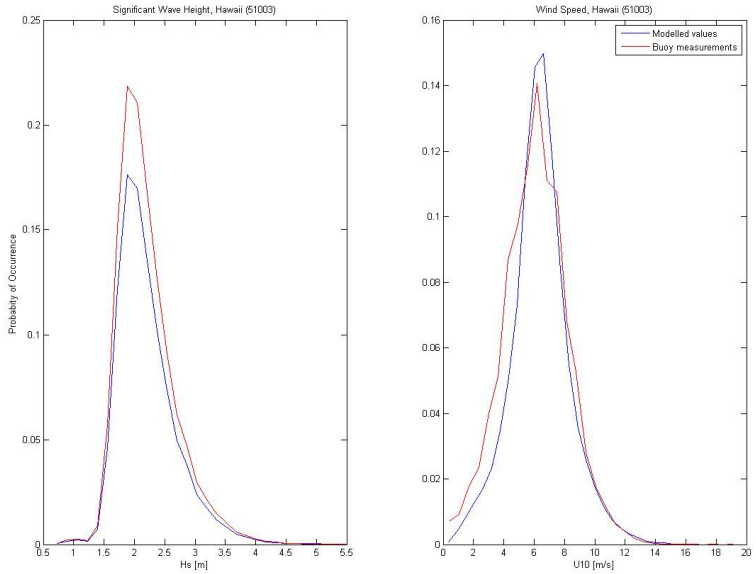

Figure 3.3 - Probability density plots for significant wave height, H_s, and wind speed at 10 m height, U_{10}, for modelled values and observations from NOAA buoy station 51003 located South of Hawaii in the Pacific Ocean. The comparison is based on hourly data for the period 1984-2003.

The distributions presented in figure 3.1-figure 3.3, show that some discrepancies exist between the modelled and observed data sets. The best overall correlation is seen for the location of buoy station 51002 south of Hawaii, figure 3.2. The modelled wind speed distribution at this point follows the observed values quite closely while the modelled wave height distribution is somewhat narrower than the observed values. In the case of the other two buoy locations larger deviations are seen.

For the location of station 51003, figure 3.3, the modelled and observed wind speed distributions are fairly similar, although the observed distribution is somewhat broader. The shape of the significant wave height distributions are comparable, however the peak of the observed distribution is notably higher.

Finally, for station 46001, figure 3.1, the modelled wave height distribution is narrower and has a higher peak than that of the buoy measurements. The wind speed at this location is generally modelled as higher than the observed values. On the whole, this location appears to be the one that has the poorest fit between the measured and observed values. It is possible that placement of the buoy 46001 might affect the results since it is located in the Gulf of Alaska relatively close to the coast and even thought the water depth is substantial, there might be external influences distorting the results.

Table 3.2 – Comparison of statistical parameters for the present climate, between modelled and observed wind speed, U_{10}, and significant wave height, H_s, distributions.

	U10: AGCM/Buoy obs.		Hs: WAM mod./Buoy obs.	
Station	Mean	Range 10^{th}-90^{th} perc.	Mean	Range 10^{th}-90^{th} perc.
46001	1.262	0.929	0.968	1.151
51002	1.043	0.845	0.987	0.625
51003	1.100	0.769	1.013	0.749
Average	1.135	0.847	0.989	0.842

Ratios for the statistical parameters describing the wind speed and wave distribution is presented in table 3.2. This comparison shows that there are notable differences between the observed and modelled data series for the present climate period. Based on the averaged differences over the tree locations, it is seen that the mean value of significant wave height is estimated very accurately by the model, with an underestimation of only 1%. The mean wind speed on the other hand, is overestimated by 13.5%. The range between the 10^{th} and 90^{th} percentile are underestimated by the models for both wind speed and significant wave height, This is consistent with the appearance of the more narrow distributions for the modelled values, presented in figure 3.1-figure 3.3.

For reference, the validation results can be compared to those presented in Mori et al. (2010), where a similar study is performed based on wind fields from the JMA/MRI-AGCM3.1 model. In that study, however, the SWAN model is used to simulate wave fields for a 20-km mesh so these values cannot be directly compared. In the validation process performed for that high-resolution study the wind fields show a better correlation with the buoy observations (for the same buoys that are used I this study) but are still overestimated by 7%.
The conclusion to be drawn from this evaluation is that there are clear uncertainties to be considered in the modelled representations of the wind and wave characteristics. Especially the inaccuracies for the wind speed is troublesome since faulty wind input to the WAM model can produce even larger error in the wave data. There also the uncertainties related to the evaluation process itself to be taken into account. With this in mind, it is still possible to estimate the ratio of change between the present and future climate which is the main focus of this study.

3.2 Numerical Computation Conditions

The numerical model used to simulate the wave fields for the present and future climate projections is as mentioned, the third-generation WAM model. The model was developed with the purpose of operational prediction of waves over the whole globe, making it well suited for this global climate study (Janssen, Günther, Hasselmann, & Zambresky, 1994). The WAM model is flexible on several points, e.g. spatial resolution, and the choice of global or regional modes with open or closed boundaries. The conditions and choices made for this simulation run will be described below.
For this study the wave climate is simulated globally, with the whole globe as one single model block, though not including the polar regions, at latitudes larger than 65^{o}N and 75^{o}S. These areas are excluded to avoid complications caused by possible interactions with the polar ice caps, when these are affected by the warming climate.
There are a number of model options that can be added to the computation conditions, if it is suitable for the study. Some of these are connected to the WAM shallow water mode such as depth refraction and current refraction mode. For this study WAM is run in deep water mode and the analysis is focused on the open ocean where the water depth is great, thus neither of the additional refraction options are enabled.
The WAM model can roughly be described, based on its three main functions: pre-processing, processing and post-processing. The pre-processing includes the designation of all time-independent information, needed for the model run and the model grid is developed from a topography data set. The input topography

information used in this study originates from the NASA Shuttle Radar Topography Mission. The spatial resolution is set to 1 degree, based on a rectangular grid of latitude and longitude.
All model constants are also pre-calculated at this stage, e.g. the surface stress dependence on wind. For the calculation of the drag coefficient, C_d, for the wind-wave interactions within the model the relationship proposed by Wu (1982) is employed. Through empirical studies, Wu showed that the drag coefficient at a given height is linearly dependent on wind speed through the following relationship (Holthuijsen, 2007; WMO, 1998; Wu, 1982):

$$C_d = \begin{cases} 1.2875 \cdot 10^{-3} & U_{10} < 7.5\ m/s \\ (0.8 + 0.0065U_{10}) \cdot 10^{-3} & U_{10} \geq 7.5\ m/s \end{cases}$$

The pre-processing programs also generate the initial wave conditions from which the model run is started. For this simulation the initial spectrum characteristics are defined based on local winds at all ocean grid points as opposed to using the same initial spectrum allover. The output from the pre-processing stage is used as setup and initial values for the subsequent processing stage.
The main processing part of the modeling sequence is naturally the most vital part of the simulation. To run the processing program, CHIEF, all time-dependent variables and user defined parameters must be defined. Also, the input wind data set, in this case the U_{10}-wind fields from the AGCM simulation, is transformed to the pre-defined model grid. Although, the input wind fields come from the JMA/MRI-AGCM3.2 which produces wind fields with a very high resolution, down to an approximate grid size of 20 km, the wind input to the WAM model is only defined for every degree latitude and longitude. The reason for this limitation is the extensive computation requirements needed for really high-resolution simulations. Since the wind parameter utilized in the WAM model is the friction velocity U_*, the wind input is transformed through $U_*^2 = C_d U_{10}^2$. Lastly, and most importantly, the transport equation is integrated over the chosen time periods of present and future climate: 1979-2003 and 2079-2099.
In the final post-processing part of the model simulation sequence, chosen output data is gathered and printed. The most important output from the model run, for the purposes of this study, is the global distribution of significant wave height. The analysis process of this parameter is described in section 3.3 below.

3.3 Statistical Analysis Methods

Because of the irregularity and randomness of ocean waves, a good way to characterise a wave climate is in terms of statistical parameterisation (WMO, 1998). For example, even though an observed wave record will never be exactly repeated, a sea-state can be said to be *stationary* if the wave distribution remains similar throughout a chosen period of time. This is a common and usually reasonable assumption when analysing shorter wave records or a single storms, but when the wave records cover years or decades, as in this study, the assumption that the conditions stay stationary clearly becomes unrealistic (Holthuijsen, 2007).

Consequently, a special approach concerning long-term statistical analysis must be employed. In contrast to short-term statistics, which are usually based on a continuous time series of surface elevations there is a need, to define parameters that, for a period of time (typically one or three hours) can represent a stationary condition (Holthuijsen, 2007). For long-term wave records the analysis is often limited to the *significant wave height*, which is also the case in this study.

The significant wave height, H_s, roughly corresponds to the wave height that can be visually observed. This useful correlation is the main reason to why this parameter has become such a widely used measurement of wave height. The significant wave height is defined as the mean height of the highest one-third of the waves in a wave record (WMO, 1998; Holthuijsen, 2007). Thus:

$$H_{1/3} = \frac{1}{N/3}\sum_{j=1}^{N/3} H_j$$

where j is the rank number based on the magnitude of the wave (with $j=1$ representing the largest wave, $j=2$ the second largest and so on), and N is the total number waves in the record. Characteristics of a wave climate can then be evaluated based on the long term distribution of the significant wave height at a given location, as well as on the return period of high values.

Contrary to short-term analysis, there is no universal theoretical model, applicable to the basic long-term statistics. Instead, assuming that the values in the data set are independent and identically distributed long-term statistics can be interpreted using extreme-value theory. Naturally the conditions for this type of theory causes problems for real wave records since subsequent values most likely are correlated. Also, since waves, although measured at the same location, can originate from many different sources, e.g. the obvious difference of swell and local wind sea, the condition of identical distribution is usually compromised as well.

The former of these complications can be controlled by using values that are sufficiently far apart in time, e.g. as in the annual-maximum approach which is described below. The latter condition is somewhat harder to manage but can be, at least partly, be satisfied by separating swell and wind sea. However, in many cases these violations against the extreme-value theory's foundation are overlooked (Holthuijsen, 2007).

There are a few different approaches by which to analyse wave statistics at a chosen location. A common first step is to visualize the full distribution of a wave record through e.g. histograms or box plots, to give an overall idea of the wave characteristics at a specific point. This first evaluation of the wave climate can for example provide an idea of what the fatigue effects on marine structures in the area will be (Holthuijsen, 2007). Since extreme values often fall outside the range of day-to-day measurements, however, fitting the data to a statistical distribution and from that extrapolate into the future is a common method to determine return periods of extreme wave heights.

The choice of a suitable statistical distribution is an arbitrary process, although experience usually limits the number of plausible candidates. For records of significant wave height the common options are the Weibull or the log-normal distribution (WMO, 1998). The initial-distribution approach has the obvious flaw of overlooking the assumption of independence of the values in a data series. In this study the full wave height distribution is analysed to evaluate local wave climate characteristics at different locations, but for the determination of return values, an approach using the yearly maxima is employed.

In order to evaluate and compare different data sets, it is important to adopt suitable methods of visualization as well as defining quantifiable parameters describing the characteristics of the distributions. A series of values of significant wave height can for example be illustrated by its probability density function, *pdf,* alternatively the cumulative density function, *cdf.* The probability density of a distribution defines the probability of occurrence of randomly drawn values from the data set. The cumulative probability density, describes the probability that a randomly chosen member of the data set will be less than a specific value.

In the analysis of local climate presented in section 4.2, both the probability density and cumulative density for the significant wave height distributions are utilized, the latter is however inversed so that the probability of exceedance is shown as a function of wave height, as opposed to the probability of non-exceedance. To demonstrate typical appearances of these functions for a record of significant wave height, figure 3.4 shows the probability density, and the cumulative density functions of non-exceedance and exceedance respectively, for a log-normal distribution.

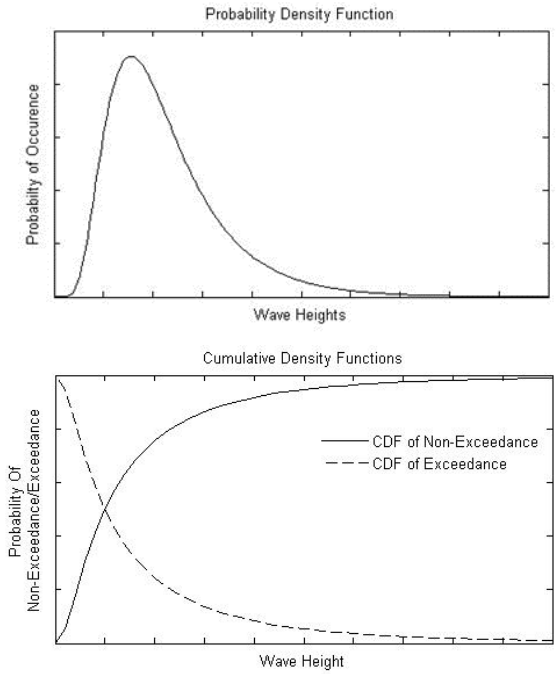

Figure 3.4 – Typical appearance of a log-normal probability density function, pdf (top) and a cumulative density function of non-exceedance and exceedance respectively (bottom).

To facilitate the comparison between the wave records for the two projected periods analysed in this study, some quantifiable and descriptive statistical parameters are used. Firstly, the mean value of a distribution gives a good indication of the overall scale of wave heights at a specific location. In order to compare the outer parts of the wave height distribution, in particular the values in the upper tail, different order percentiles are used. A percentile represents a value below which a specified percentage of the values of a distribution are located. If ξ, is a stochastic variable with the probability density function, F, the meaning of the p^{th} percentile is the value of, q_p, which solves the equation $F(q_p) = p/100$, and thus p% of the values of the distribution is smaller than q_p (Vännman, 2002).
Finally, it is valuable to have a measurement of the range of values in a certain distribution. In this study the spread between different percentiles are found useful to describe the appearance of a distribution. The differences between the 25^{th} and 75^{th}; the 10^{th} and 90^{th} and the 2.5^{th} and 97.5^{th} percentiles are therefore used in order to indicate the range of the distributions, thus including 50%, 80% and 95% of the data set values respectively. The range between the 25^{th} and 75^{th} percentile is commonly known as the *quartile deviation* and the other two range measures will hereafter be called the *80%-range* and *95%-range* for simplicity (Vännman, 2002). The reason for not simply using the full range, from the

minimum to the maximum value is due to the outlier values which are common in wave height records.

As mentioned, the evaluation of return values and corresponding periods for large wave heights is, in this study based on the annual-maximum approach. According to extreme-value theory the maxima of a population containing random values belong to the *generalised extreme-value distribution (GEV).* Moreover, if the parent distribution is either the Weibull or the log-normal distribution, which is usually the case for records of significant wave height the three parameter GEV distribution reduces to the two parameter Gumbel distribution (Holthuijsen, 2007). This is the foundation of the mentioned, *annual-maximum approach* for long-term statistical analysis which is used in this report to determine return periods for extreme waves in different locations. The advantage of this approach is that the condition of independent values is fulfilled since only one value per year is considered. On the other hand, this method drastically decreases the number of values on which the analysis is founded. The wave records of 25-years for each period, available for this study, are judged sufficiently long for this type of analysis (a minimum of five years data is recommended by the WMO (1998)).

3.3.1 Fitting Data to a Statistical Distribution

As has already been stated, the fitting of a data set to a statistical distribution is basically an arbitrary process which can never be fully objective. There is no general rule for deciding which statistical distribution is most suitable for a specific data set, which is a major weakness of the method (WMO, 1998). The bias in the fitting process also induces uncertainty issues which must be considered during the evaluation of the results. This is especially important when extensive extrapolation is conducted, which is often the case when calculating return values and return periods for extreme waves.

There are three possible forms of extreme value distributions to which data can be fitted. These are commonly known as the *Fréchet*, *Gumbel* and *negative Weibull* extreme value distributions. The tree-parameter *Generalized Extreme Value* distribution, which is used in this study, has the advantage of combining all tree distribution shapes into one. The GEV for annual-maxima (*am*) can be expressed by:

$$\Pr\left\{\underline{H}_{s,am} \leq H_{s,am}\right\} = e^{-\left(1+k\frac{H_{s,am}-\mu}{\sigma}\right)^{-1/k}} \qquad \sigma > 0$$

where μ is the location parameter, determining the location of the distribution on the H_s-axis; σ is the normalisation or scaling parameter, determining the width of the distribution and *k* is the shape parameter.
The three possible shapes contained in the GEV distribution depend on the sign of shape parameter, k. For k>0 the GEV turns into the Fréchet distribution, for k<0, the shape is that of the negative Weibull and lastly, if k=0 (interpreted as k→0) the distribution is reduced to the Gumbel shape (Reeve, 2011). The main difference of the three shapes is in the characteristics of the tail of the distribution. While the negative Weibull distribution has an upper end point, the two others do not, but have tails decaying, exponentially for Gumbel and polynomially for Fréchet.
Since significant wave height data sets are likely to belong to either the Weibull or the log-normal distributions the most probable fit for the annual-maxima is, according to the extreme value theory, the Gumbel shape of the GEV (Holthuijsen, 2007). This shape is as mentioned, acquired when the shape parameter, *k,* of the GEV comes close to zero. The Gumbel distribution can be expressed through:

$$\Pr\{\underline{H}_{s,am} \leq H_{s,am}\} = e^{-e^{-\frac{H_a-\mu}{\sigma}}} \quad \sigma > 0$$

with location parameter, μ, and scaling parameter, σ.
There are different techniques that can be used to find the best possible fit between a data record and a chosen distribution. Commonly used are e.g. *least-square fitting* which minimises the sum of the squared differences between the data set values and the chosen distribution, or the *maximum-likelihood technique* which maximises the probability that a value from the data record belongs to the candidate distribution (Holthuijsen, 2007).
In this study the annual-maxima of the significant wave records for chosen locations are fitted to the GEV distribution by means of maximum likelihood. As could be expected, it is found that the distributions resemble the Gumbel shape, which is thus the distribution that is used for the evaluation of return values. For the Gumbel distribution, the maximum likelihood estimators of the distribution parameters, $\hat{\mu}$ and $\hat{\sigma}$ can be calculated numerically through the following two equations (WMO, 1998):

$$\hat{\mu} = -\hat{\sigma}\log\left[\frac{1}{n}\sum_i exp\left(\frac{-h_i}{\hat{\sigma}}\right)\right]$$

$$\hat{\sigma} = \frac{1}{n}\sum_i h_i - \frac{\sum_i h_i exp\left(\frac{-h_i}{\hat{\sigma}}\right)}{\sum_i exp\left(\frac{-h_i}{\hat{\sigma}}\right)}$$

Whatever technique is employed, every fitting needs to be visually examined to ensure the agreement between the data set and the statistical distribution, especially for the upper tail of the distribution which usually contains fewer values than the heavy lower tail.

When a series of annual-maxima has been successfully fitted to a statistical distribution the result can be extrapolated into the future in order to evaluate return periods for high values of wave heights that fall outside the range of the original data set. To determine the return period (in years) from a record based on the annual-maximum approach the following relationship can be used (Holthuijsen, 2007):

$$RP_{\underline{H}_{s,am}>H_{s,am}} = \frac{1}{1 - Pr\{\underline{H}_{s,am} > H_{s,am}\}}$$

where $Pr\{\underline{H}_{s,am} > H_{s,am}\}$, is the cumulative distribution function for the fitted data set. As part of this study the annual-maxima at chosen regions will be fitted to the Gumbel distribution and the 50- and 100-year return values will be calculated. These values thus correspond to a wave height that statistically, will be exceeded only once every 50 respectively 100 years. There are always uncertainties involved when extrapolating of a distribution is employed. This must be kept in mind when calculating return values, especially for higher return periods.

4 Results and Discussion

In the following chapter the results from the analysis and comparison between present and future wave climates will be explored. To some extent, and for comparative purposes, the wind fields from the AGCM climate simulations will also be examined as part of the analysis. Quantitative assessment of changes in wind fields and wave climate respectively is thought to give a deeper understanding of the impacts of climate change.

Initially, in section 4.1, a global analysis is presented, comparing the averaged wave and wind climates of the two periods. The aim of this assessment is to give an overview of the daily wave climate on a global scale, as opposed to extreme climates which usually call for regional or local evaluations. Both yearly averages and seasonal differences are studied.
In the second subsection, 4.2, a comparison of local wave climates is implemented at a few chosen locations. In the same way, as for the global scale, both yearly distributions and seasonal irregularities are of interest on the regional scale. The locations that are analysed are chosen with the hope of giving an overview of a range of possible different wave climate developments and characteristics.
In section 4.2.1, the annual maximum values of the significant wave height series, at the chosen locations, are evaluated based on extreme value theory. The annual maxima are fitted to the Gumbel extreme value distribution and return values for 50- and 100-year waves are calculated.

4.1 Global Distribution of Averaged Values of Wind Speed and Significant Wave Height

The main aim of this section is to give an overall impression of global distribution patterns of average wind speeds and wave heights and their relative scale. It is important to underline the crudeness of the results presented in this section, since they are based on averages of wave characteristic for periods as long as 25 years. Consequently possible trends within the data record of one climate period will not be acknowledged.
On the other hand, the period averaged values of significant wave height make potential large-scale shifts between the two climate periods very clear which is the second and most important aim of the study. The wave climates of the two periods are thus put in relation to each other making it possible to identify changes and pin them to different regions as well as time of year.
The averaged values presented in this section are calculated based on the hourly wind speed, U_{10}, and significant wave height, H_s, at every grid point. The parameters averaged counterparts are denoted by, $\overline{U_{10}}$, and, $\overline{H_s}$, respectively.

4.1.1 Global Distribution of Averaged Wind Fields from the AGCM Simulation

In figure 4.1, the spatial distribution of the period averaged wind fields from the AGCM simulation is presented. The top part of the figure contains the result for the present climate (1979-2003) and the bottom part the wind field simulated for the future period (2075-2099).

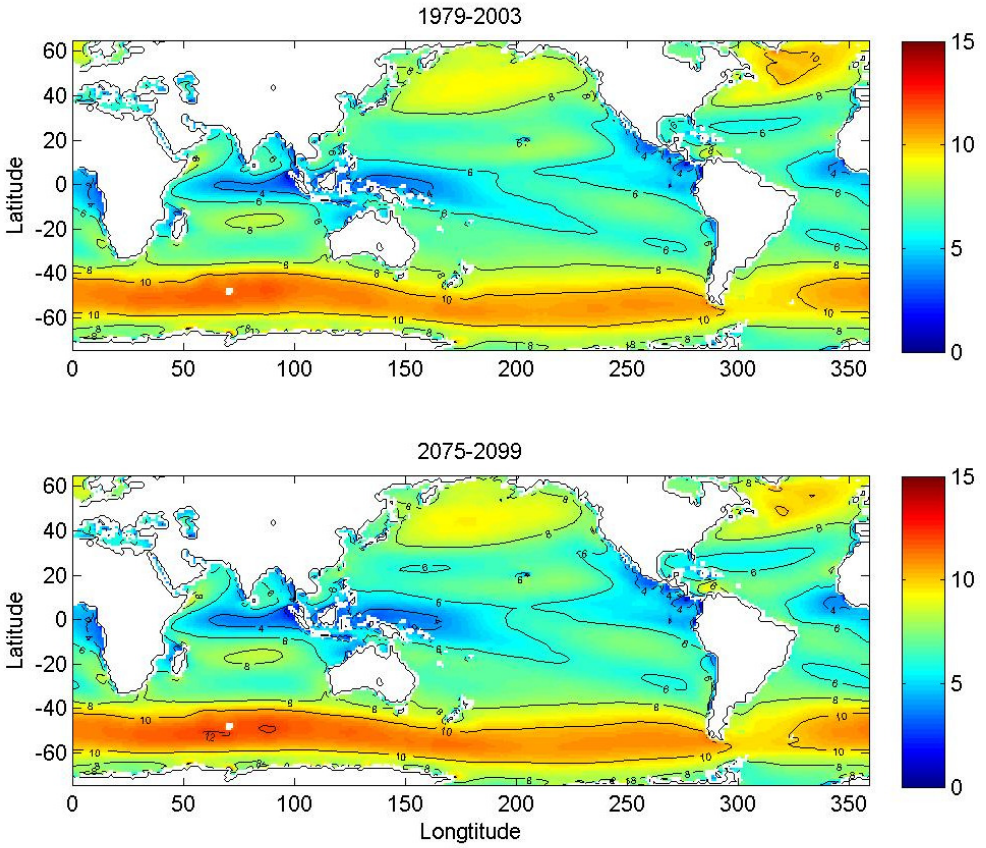

Figure 4.1 – Global distribution of wind speed (m/s), simulated by the JMA/MRI-AGCM climate model. The result is based on the 25-year average for the periods 1979-2003 (top) and 2075-2099 (bottom).

Figure 4.1 clearly illustrates a strong latitude dependence of the average wind speed distribution. The largest wind speeds (approximately 10 m/s and above) are experienced in the high-latitude regions of the Southern Indian, Pacific and Atlantic Oceans as well as in the Antarctic Ocean. Furthermore, wind speeds of up to 10 m/s are seen in the northern parts of the Pacific and Atlantic Oceans.

The average wind fields in the mid-latitude regions, both north and south, are slightly smaller, ranging from 6-8 m/s. The calmest wind conditions are found in the equatorial region e.g. around the Indonesian archipelago and of the west coast of Central America.

One thing that is important to keep in mind, when analysing climate data of any kind, is that the processes behind average climate characteristics, as shown figure 4.1, and extreme events differ significantly. Thus, it is not possible to draw any

direct conclusions about the distribution of maximum wind speeds, exclusively based on the result shown in figure 4.1. In fact, areas which are affected by extreme climate events such as tropical cyclones for example, often show quite modest average wind speeds.

One example of this phenomenon is the area south of Japan in the Pacific Ocean, which is known to experience quite frequent tropical cyclones, but where the average wind field show no sign of such activity (see figure 4.1 around latitude 30^{o}N and longitude 120-140). Other areas that show these characteristics are the area off the North American east coast as well as other mid-latitude regions in both the Northern and Southern Hemisphere.

Figure 4.1 also shows that the overall spatial distribution pattern of averaged wind speeds remains relatively similar between the simulations of the present and future climate. However, the magnitude of the wind speeds change in many places between the two periods. To elucidate these quantitative transformations of the wind climate, the change between the two periods is plotted in figure 4.2. The change is expressed both in meters per second (upper figure) and as normalized percental change.

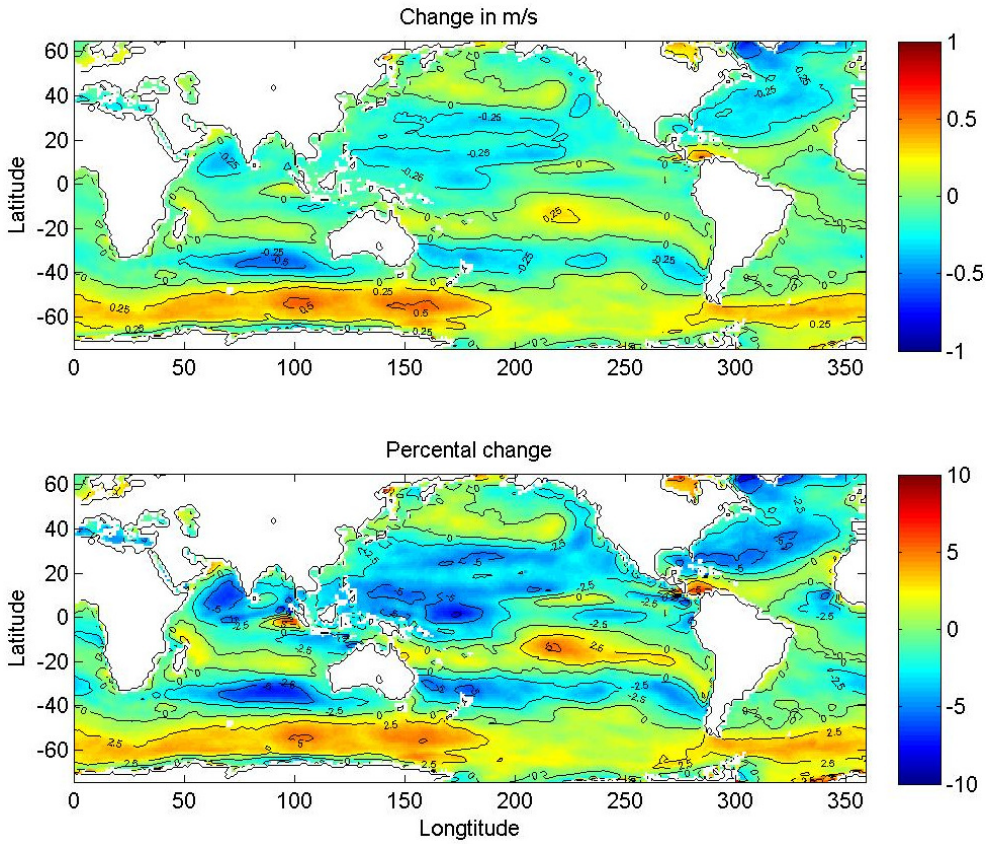

Figure 4.2 – Change of the 25-year averaged global wind speed between present (1979-2003) and future (2075-2099) climate simulations. The top figure shows the change, expressed in meters per second, and the bottom figure is based on the normalised change between the two periods, expressed in percent.

The largest increases of the period averaged wind speed are observed in the region around latitudes 50-70°S, however excluding the Pacific Ocean, where the change attains levels in the order of 2.5-5%, corresponding to approximately 0.25-0.5 m/s. The area just south of the equator is the least affected of the changing climate according to the simulations, as is the high-latitude regions of the Pacific Ocean.
Several areas, e.g. the equatorial region in the Pacific Ocean and the west and central parts of the northern Atlantic Ocean, experience a decrease of wind speeds 2.5-5% (≥0.25 m/s), locally even larger decreases may occur.

4.1.2 Global Distribution of Averaged Wave Climate from the WAM Model

The aim of this subsection is, in likeness to the previous analysis of wind fields, to give an overview of the spatial patterns related to the global distribution of significant wave height, as well as to evaluate and locate possible changes between the present and future climate. In figure 4.3 the period averaged distribution of significant wave height, numerically modelled by the WAM model, is presented for the present (top) and future climate (bottom).

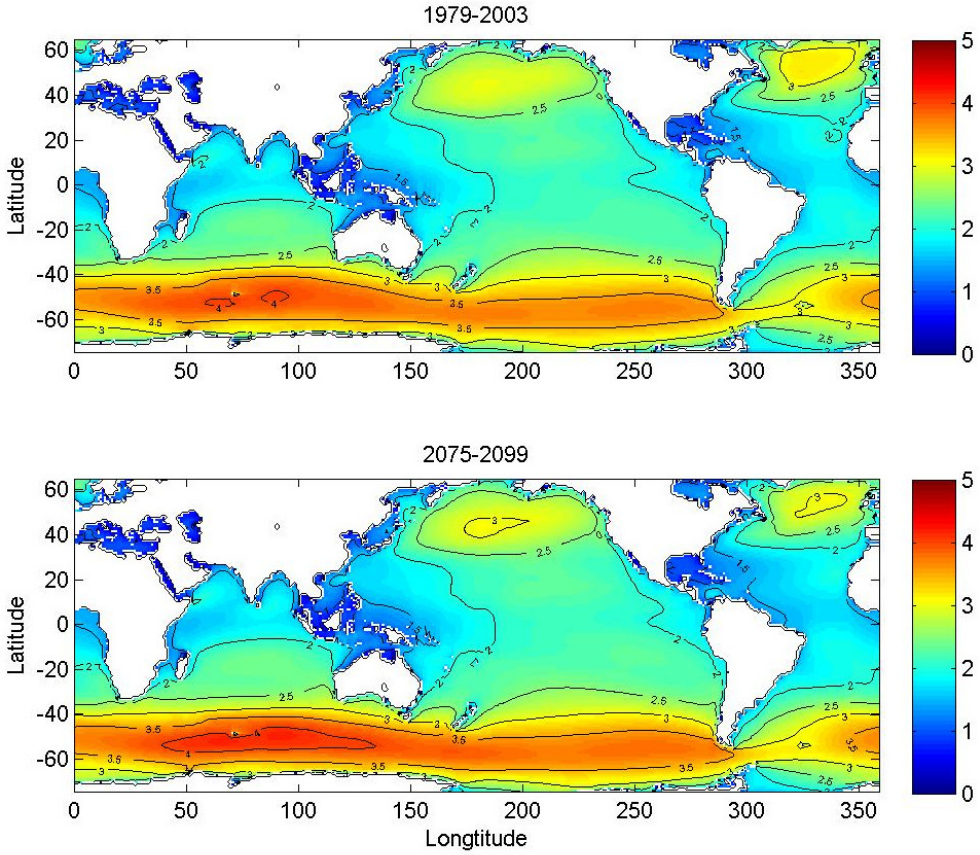

Figure 4.3 - Global distribution of significant wave height (m), simulated by the WAM model. The result is based on the 25-year average for the periods 1979-2003 (top) and 2075-2099 (bottom).

The spatial distribution of the significant wave height is, as might be expected, similar to that of the wind field averages presented figure 4.1. This mean the largest waves are found in mid to high-latitude areas, approximately around 40°N-60°N and 40°S-70°S respectively. The Southern Hemisphere experiences the highest values with average wave height of up to almost 5 m, compared to

regional maximums of approximately 3m in the northern Pacific and Atlantic Oceans.
There is quite obviously a strong latitude dependence related to the average wave height. In accordance to the patterns found for wind speed in the previous section, two bands of prominent wave heights can be identified in the high latitude regions of both hemispheres. In figure 4.4 this phenomenon is made even clearer, by showing of the global average values of significant wave height from north to south.

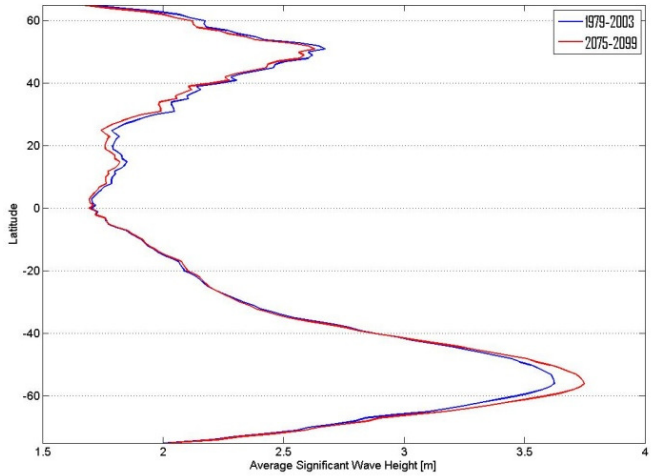

Figure 4.4 – Illustration of the latitude dependency of the averaged significant wave height. The latitudinal average of the wave height field, presented in figure 4.2, is plotted on the horizontal axis, against the latitude range of 75°S-65°N on the vertical axis.

In this figure the southern and northern high-latitude peaks are easily recognized, as is the low wave region around, and immediately north of the equator. The result presented in figure 4.4 also indicates that the largest changes of the period averaged significant wave height, from present to future climate, occur in the Southern Hemisphere around latitudes 50°S-60°S. The changes in the Northern Hemisphere is not nearly as obvious, though a general decrease in significant wave height is indicated. The complete global distribution of the change in wave climate between the two periods is illustrated in figure 4.5 below. In the same way as in figure 4.2 the top graph show the averaged change in meters while the lower figure demonstrates the normalized change in percent.

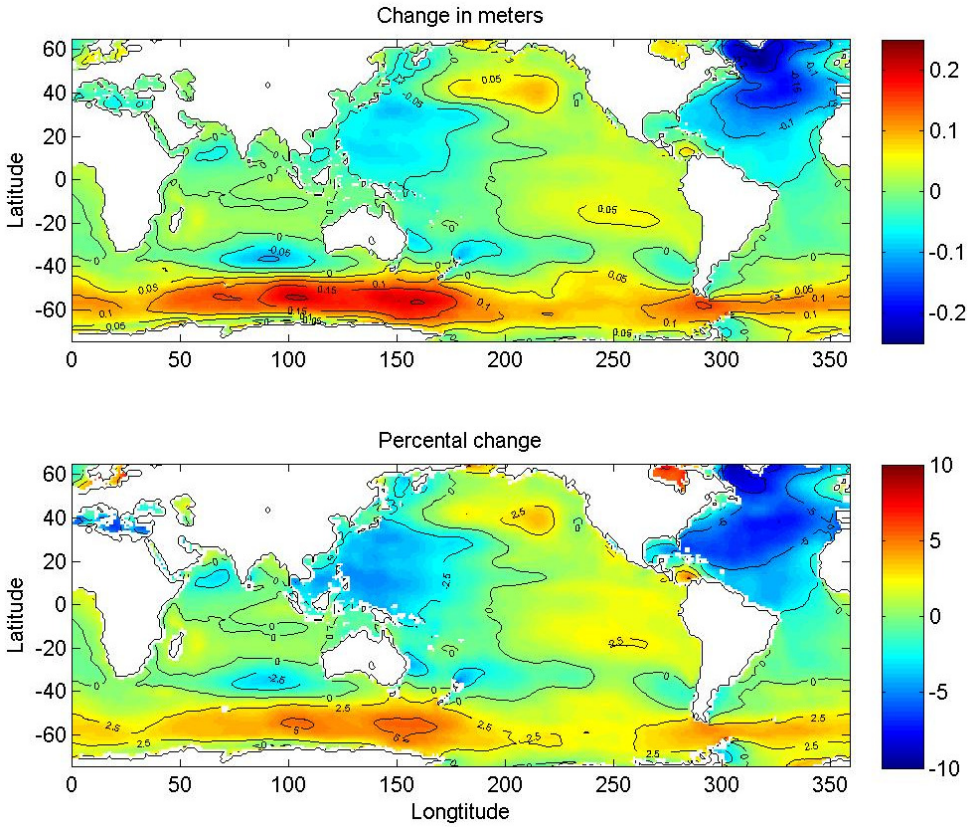

Figure 4.5 - Change of the 25-year average of global significant wave height between present (1979-2003) and future (2075-2099) climate simulations. The top figure shows the change, expressed in meters, and the bottom figure is based on the normalised change between the two periods, expressed in percent.

Comparing the percental changes of wind speed and wave height, in figure 4.2 and figure 4.5 respectively, shows a generally analogous result. However the wave fields seem to experience slightly larger changes than the wind fields, in the high wind speed/wave height regions of the mid to high latitudes. This larger sensitivity of the wave field might be explained by the fact that wave height is proportional to square of the wind speed.

The largest increases are, like before located in the Southern Atlantic, Indian and parts of the Pacific Ocean as well as in the Antarctic Ocean. In this region the changes in average significant wave height locally reaches levels of up to over 5%, and increases above 2.5% is wide. Compared to the change in wind speed the areas of large increases are considerably more extensive. Also noticeable is the large area of significantly lower future wave heights in the North Atlantic Ocean. A

considerable part of this region shows decreases of 5% and above (much more far-reaching changes than for wind speed).
Interestingly, the north western region of the Pacific Ocean, the tropical cyclone intense area off the coast of Japan, shows a clear decrease of the mean significant wave height. As mentioned in section 2.2.3 there are studies that show that tropical storms are likely to increase in the region, in a future warmer climate. It is therefore once again meaningful to point out the fundamental differences of the processes creating the daily average climate and the processes behind extreme events. Thus these phenomena should always be analysed and evaluated separately.

4.1.3 Seasonal Effects on the Distribution of Global Average Significant Wave Height

In many parts of the world the wave climate and the magnitude of waves are strongly dependent on the time of year. Figure 4.6 illustrates the distribution of the period averaged significant wave height, in a similar manner as in figure 4.3. Yet, the distributions represented below are based on the seasonal averages, in contrast to yearly averages which were analysed above.
The years have thus been divided into four periods: *winter season* from December to February; *spring season* from March to May; *summer season* from June to August and *fall season* from September to November. Inevitably, this division will not fully satisfy seasonal changes in every part of the world (and the naming of the seasons would naturally be the reverse if based on the calendar in the Southern Hemisphere) but based on the monthly distributions this grouping of months is judged to best represent the yearly variations on a global scale (see Appendix A for monthly distributions).

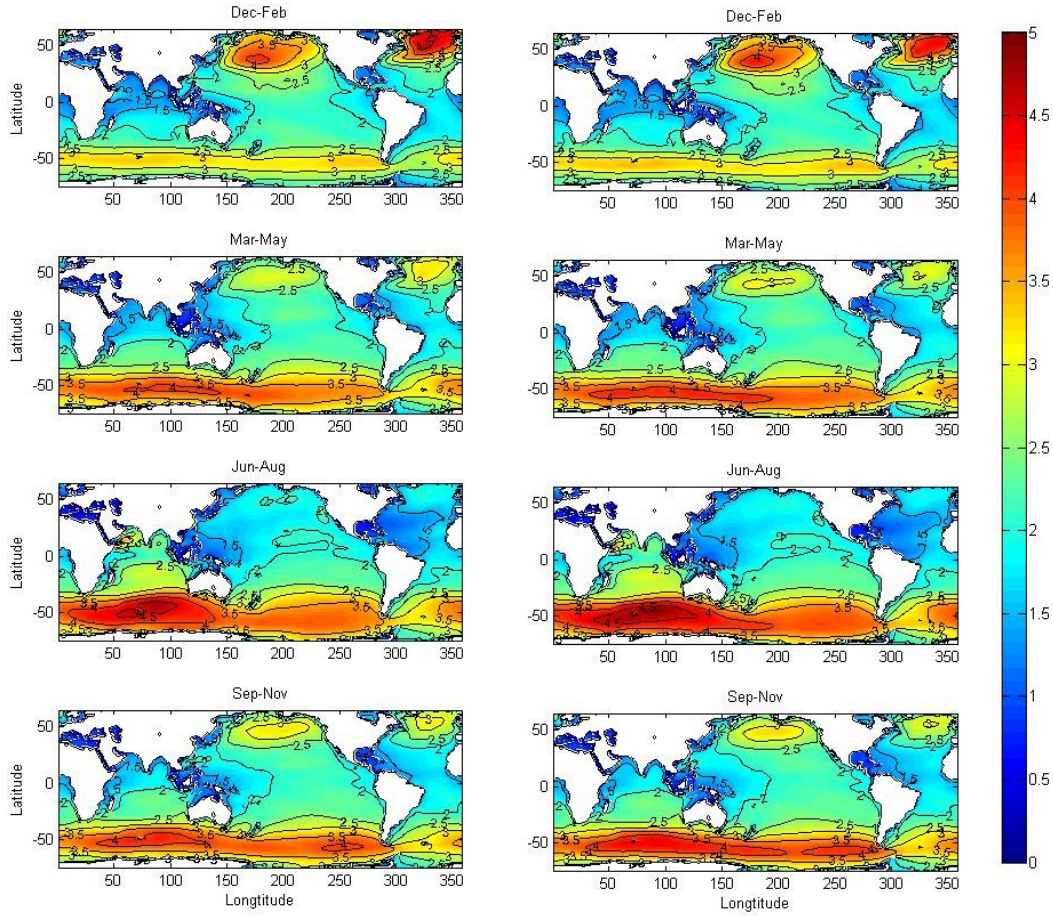

Figure 4.6 – Global distribution of the period averaged significant wave height (m) for four seasons, winter, spring, summer fall. The seasons are defined as the periods: December-February, March-May, June-August and September-November, respectively. The left-hand side figures show the result for the present climate simulation and the right-hand side represents the future climate.

The seasonal pattern illustrated in figure 4.6 shows that wave heights tend to be higher during the winter period in many parts of the world, i.e. from December to February in the Northern Hemisphere and from June to August in the southern part of the globe. The wave climate in the equatorial region remains fairly constant throughout the year. During spring and fall the simulated wave fields are quite similar to those of the yearly average, pictured in figure 4.3. This is to be expected since these seasons represent the transitional periods between the two extremes of the averaged climate: winter, when the Northern Hemisphere reaches

maximum wave heights and the Southern Hemisphere's wave fields are at their lowest, and summer when matters are reversed.
In the figure 4.7 below, the latitudinal distributions of averaged wave height for the different season are represented.

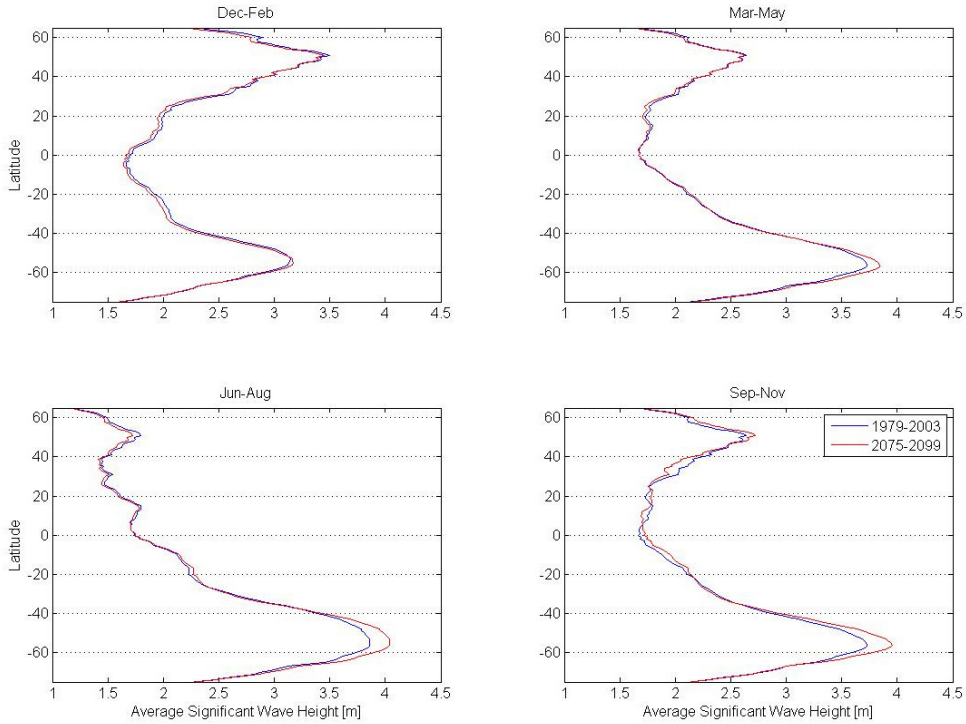

Figure 4.7 - Illustration of the latitude dependency of the averaged significant wave height based on the global, seasonal distributions. The latitudinal average of the wave height field, presented in figure 4.6 is plotted on the horizontal axis, against the latitude range of 75ºS-65ºN on the vertical axis.

During most of the year (spring, summer and fall), the Southern Hemisphere presents noticeably higher wave heights than the northern part of the globe, with really large differences in summer. During winter, however, these differences are evened out. It is clear, from these graphs, that seasonal alterations of significant wave height affect the Northern Hemisphere, especially the high-latitude region, in a much larger extent than any other part of the world.
While the latitudinal average wave height at latitude 50ºN varies from a low approximate 1.7 m in summer to a maximum of approximately 3.5 m in winter, a total of just under 2 m difference, the southern equivalent variation at latitude 50ºS is of a mere 3.2 m in winter to just under 4m in summer, a total of under 1 m

seasonal difference. Figure 4.7 also illustrates the stationary nature of the equatorial region which is hardly affected by seasonal changes and shows wave heights of approximately 1.5-2 m all year around.
Changes between the present and future values of significant wave height can also be seen in figure 4.7. According to the latitudinal averages the largest increases will occur in the high-latitude region of the Southern Hemisphere, especially in the summer and fall seasons. The differences between the periods are significantly smaller in the Northern Hemisphere, but overall, a small decrease in wave height is indicated throughout most of the northern latitudes. A slight decrease of the equatorial wave height during winter is also visible. The full global distribution of the changes between present and future climate is presented in figure 4.8 below.

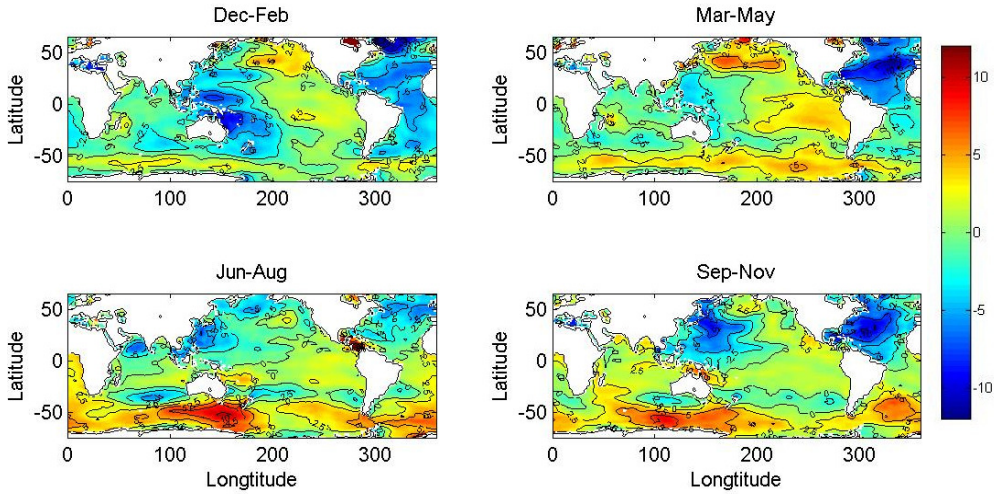

Figure 4.8 - Change of the 25-year average of global significant wave height based on the seasonal distributions, between present (1979-2003) and future (2075-2099) climate simulations. The top figure shows the change, expressed in meters, and the bottom figure is based on the normalised change between the two periods, expressed in percent.

The changes in averaged significant wave height throughout the period December to February are pretty minor in large parts of the world. There are however, areas such as most of the Atlantic Ocean as well as the western Pacific Ocean which show quite significant decreases of wave height, ranging from 2.5 to as much as 10% in some areas. A slight increase of wave heights in the proximity of the Gulf of Alaska is also visible.
Spring season presents notable increases of wave heights in the North Pacific Ocean by up to 5%. Increases are also experienced along in the southern parts of the Indian and Pacific Oceans as well as in an area west of the South American

continent. A significant decrease of the wave fields in the northern Atlantic Ocean, ranging from 5 to more than 10% can also be seen.
During summer season large increases of wave height are shown in the Southern Hemisphere. Largest are the increase south of Australia and New Zeeland where, locally, the change is more than 10%. Further increases, of approximately 2.5-5%, are found in the southern and east South Atlantic Ocean. In the northern high-latitude regions the significant wave heights tend to become somewhat lower in the future, while most of the equatorial remain quite unaffected.
Finally, fall season show continuously large increases in the high-latitude regions of the Southern Hemisphere. Large areas in the Northern Hemisphere experience reduced wave heights, especially in the western parts of the North Pacific and North Atlantic Oceans.

4.2 Local wave climate

The large scale changes that are discussed in the previous section are dependent on changes of atmospheric pressure and wind fields. Other, small-scale processes are, however involved when analysing daily wave climate on a regional scale. In order to evaluate local differences of wave characteristics, a few locations spread over the world are chosen. Due to the limited resolution of the model run in this study, the chosen locations are located in deep water in open ocean, in order to minimize interference from bottom friction and similar disturbances.
The locations for these points are selected based on the premises that they represent areas where changes are found to be prominent, according to the results shown in the previous section. In addition, there are a few points which have been chosen to represent areas with other characteristics i.e. point 1, located in an equatorial region in the Indian Ocean as well as point 4, located south west of Japan representing an area which experiences tropical storms. The locations of points 5 and 6, in the North Pacific Ocean, are chosen at the positions of two of the NOAA buoys used in the model performance evaluation in section 3.1. In total, ten points are selected for further examination and their positions are visualized and defined in figure 4.9 and table 4.1 below.

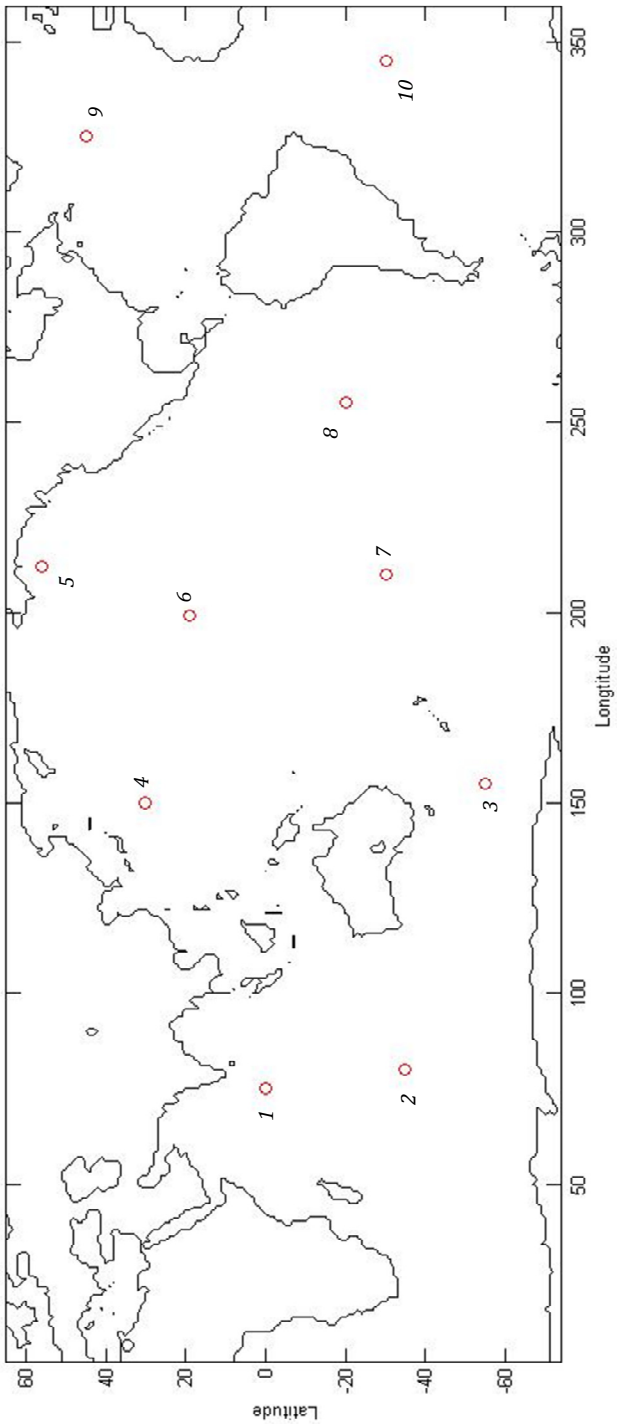

Figure 4.9 – Visualization of the locations which are analysed in the evaluation of local wave climate, presented in this section.

Table 4.1 – Spatial locations and brief descriptions of the ten locations, chosen for further study of the local wave climate.

Point	Latitude	Longitude	Location, notes
1	0	75 E	*Indian Ocean, on the equator*
2	35 S	80 E	*Southern Indian Ocean*
3	55 S	155 E	*South of Australia/New Zeeland*
4	30 N	150 E	*South-east of Japan, region of tropical storms*
5	56 N	148 W *(212)*	*Gulf of Alaska, position of NOAA buoy 46001*
6	19 N	161 W *(199)*	*Hawaii, position of NOAA buoy 51003*
7	30 S	150 W *(222)*	*South Pacific Ocean*
8	20 S	105 W *(255)*	*South-Eastern Pacific Ocean*
9	45 N	35 W *(325)*	*North Atlantic Ocean*
10	30 S	*15 W (345)*	*South Atlantic Ocean*

In the following subsections the wave climate of each of the chosen location will be analyzed and compared for the simulated present and future climates. An initial overview of the characteristics of each location is given in figure 4.10, in the form of boxplots. The boxes represent the quartile deviation range of the wave distributions with the central red line corresponding to the mean value of the significant wave height for the defined location and time period.

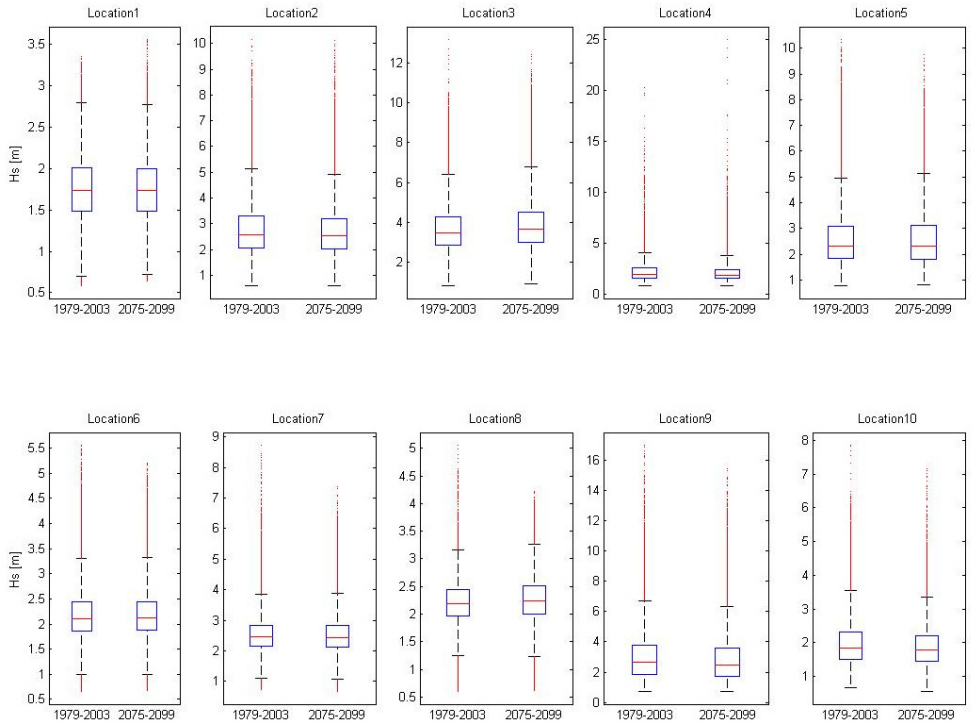

Figure 4.10 – Boxplot chart for all the chosen locations defined in figure 4.9 and table 4.1. The outer limits of the boxes show the innermost 50% of the wave height distributions and the red line signifies the distribution mean value. The whiskers cover the range from $q_{25} - 1.5(q_{75} - q_{25})$ *to* $q_{75} - 1.5(q_{75} - q_{25})$ *where* q_{25} *and* q_{75} *are the 25th and 75th percentiles respectively. Values falling outside this range are plotted as outliers (red dots).*

Additionally, the whiskers connected to the boxplots define a range of wave heights with lower limit, $q_{25} - 1.5(q_{75} - q_{25})$, and upper limit $q_{75} - 1.5(q_{75} - q_{25})$ where q_{25} and q_{75} are the 25th and 75th percentiles respectively. Values that fall outside these limits are considered outliers (red dots) in the diagrams.

Based on this overview it is clear that appearance of the wave distributions differ quite widely depending on location. Note for example location 1, placed in the equatorial region of the Indian Ocean, which shows a fairly even distribution of relatively low wave heights. Location 4, on the other hand, is situated off the coast of Japan in a region affected by tropical storms. The wave height distribution at this location has a completely different appearance, with a quite compact main distribution, but with a long tail of individual, very high waves of up to 20-25 meters.

In figure 4.1 to figure 4.20, the characteristics of the simulated wave height distribution are visualized for each point respectively. The left-hand side of the figures (plots *a* and *b*) show the monthly average values and monthly maximum of

the significant wave height, plotted for the two 25-year periods of interest. For reference, the mean value and 90th percentile value of the monthly data series are marked in the diagrams (dashed and dash-dotted lines for mean and 90th percentile values respectively).

It must be noted that the graphs of monthly maximum values are presented here, only for reference purposes, and to give an indication if the magnitude of large waves at a location as well giving an indication of increases/decreases from present to future climate. To make a full analysis for maximum values, taking into account phenomena such as tropical storms and other extreme events, a model with a higher resolution is recommended (Mori, Yasuda, Mase, Tom, & Oku, 2010).

The upper right-hand figures show the empirical cumulative density function of exceedance, *cdf,* for the modelled significant wave height for every third hour. These plots state the probability that a certain randomly chosen value of significant wave height is exceeded. The lower right-hand figures contain the distribution's probability densities, *pdf*, calculated for values every 0.1 m, and which show the probability of occurrence for a certain wave height. In both figures the blue lines corresponds to present climate and the red lines to future climate.

The values of the statistical parameters, presented in section 3.3, are frequently used as reference in the following text and are summarized in table 4.2 and table 4.3. The mean value of the data set as well as the 25th, 50th (median), 75th, 90th and 99th percentiles are found in table 4.2, and are intended to help quantify and describe the wave height distributions and changes between periods in and functional manner. All values presented in the table are calculated from wave heights for every third hour at each point. In addition, three measures of the range of the distributions are found in table 4.3. These are the quartile deviation and the 80% and 95%-range measures which were defined in section 3.3.

Point 1 – Equatorial Region South of India, Indian Ocean

The first chosen location lies on the equator just south of the Indian peninsula. The point is chosen to represent the wave climate characteristics of an equatorial region where, based on the analysis in the previous section, the seasonal changes are small and the present and future climate distribution of significant wave height are expected to be relatively similar.

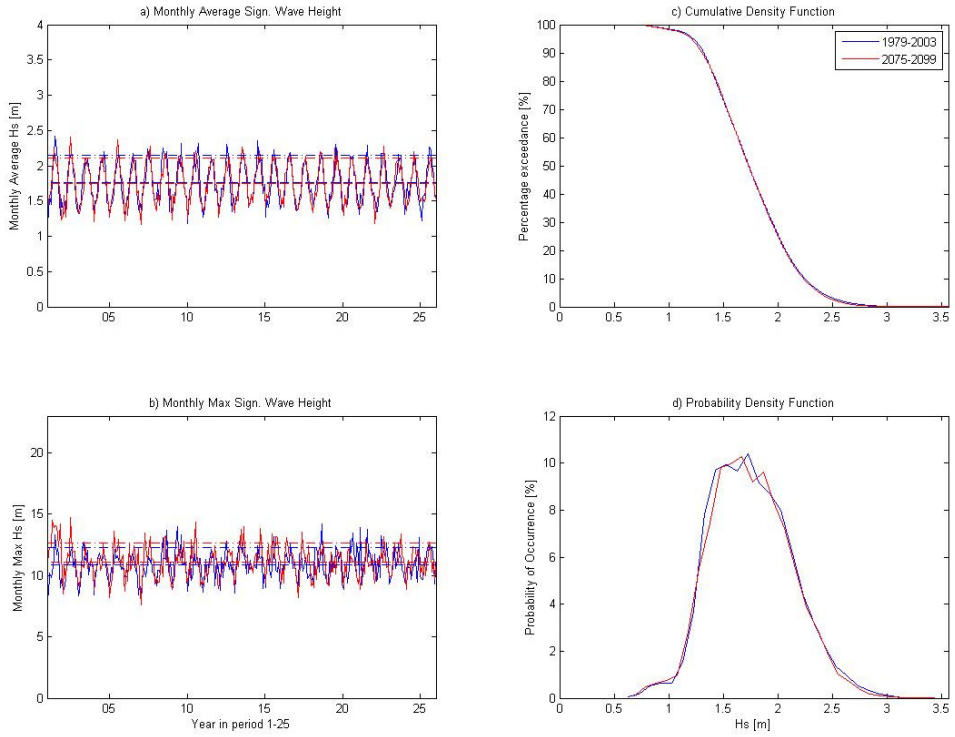

Figure 4.11 – Characteristics of the local wave height distribution of location 1. a) Series of monthly averaged significant wave height for the present and future climate simulations. b) Series of the monthly maximum significant wave height for the present and future climate simulations. In figures a-b, the mean value and 90th percentile value of the monthly data series are marked in the diagrams by dashed and dash-dotted lines respectively. c) Cumulative density function of the significant wave height for every 3rd hour. The probability of exceedance is plotted against the significant wave height. d) Empirical probability density function of the significant wave height for every 3rd hour. The probability of occurrence is plotted against the significant wave height.

As expected, the wave measurement series presented in figure 4.11a, indicates a wave climate with small seasonal variation. The 95%-spread of the distribution only measures approximately 1.4 m (see table 4.3) around a mean value of 1.8 m. Figure 4.11c-d also confirms the similarity of the wave height distributions for the present and future climate simulations, with the biggest difference between the

two periods being the 2.4% decrease of the 99th percentile value, corresponding to about -6 cm. Worth noting is that, the monthly maximum values for the future climate simulation appears to be larger than for the present climate, while the average monthly values, as mentioned remain the same.

Point 2 – Southern Indian Ocean

In the same way as for point 1, the fundamental characteristics of point 2, located in the southern Indian Ocean is presented in figure 4.12. The wave characteristics at this location clearly depart from those of the equatorial region presented above.

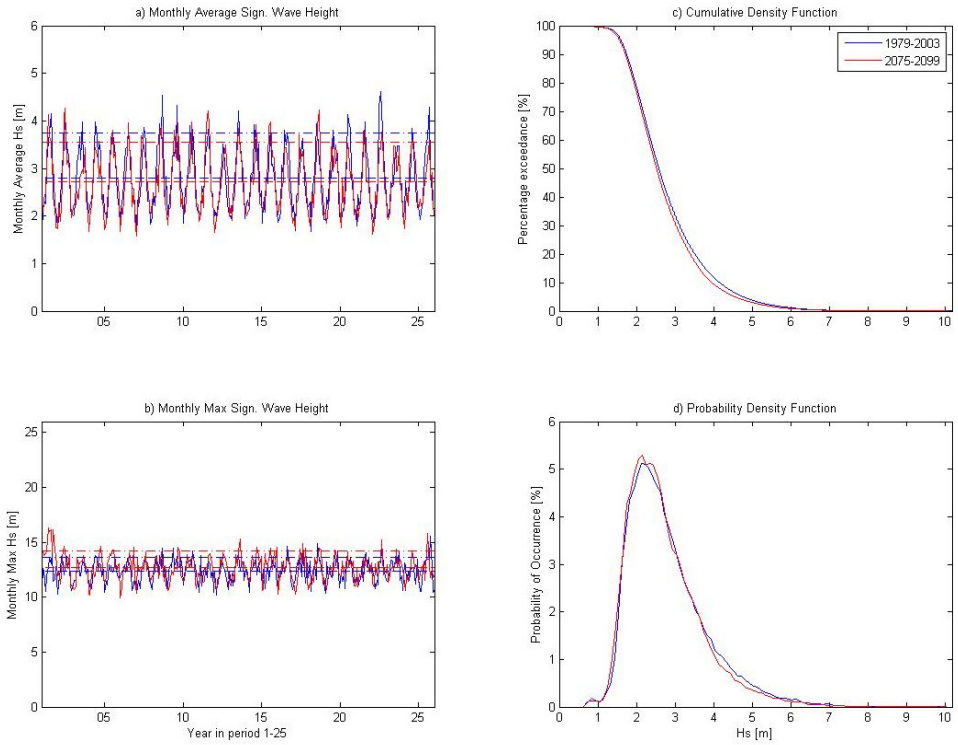

Figure 4.12 - Characteristics of the local wave height distribution of location 2. a) Series of monthly averaged significant wave height for the present and future climate simulations. b) Series of the monthly maximum significant wave height for the present and future climate simulations. In figures a-b, the mean value and 90th percentile value of the monthly data series are marked in the diagrams by dashed and dash-dotted lines respectively. c) Cumulative density function of the significant wave height for every 3rd hour. The probability of exceedance is plotted against the significant wave height. d) Empirical probability density function of the significant wave height for every 3rd hour. The probability of occurrence is plotted against the significant wave height.

Initially, it is noted that the mean wave height at this point is remarkably higher, at 2.8 m and 2.7m respectively for the two periods. The 99th percentile of the distribution take on a value as high as approximately 6 m, providing an indication of the higher waves in of the distribution. In addition, figure 4.12a, indicates that the seasonal variations are relatively large in this region. In table 4.3, the value of the 95%-spread is stated as 3.9 and 3.7 m for the two periods, thus also identifying a decreasing variation of wave height of more than 5%, which corresponds to 20 cm.

Figure 4.12c and d, show that there is an overall decrease in significant wave height from the present to future climate, especially for wave heights of the upper half of the distribution (the median value of the distribution is approximately 2.5 m). This is confirmed in table 4.2, where all stated percentile values show decreasing values for the future climate simulation. The largest reduction is that of the 90th percentile which decreases by 5%, or approximately 20 cm. Similarly to the wave record for point 1, figure 4.12 show an increase of monthly maxima from the present to the future climate simulation.

Point 3 – South of Australia and New Zeeland

The third location is situated between and south of Australia and New Zeeland. According to the global analysis in section 4.1.2, this is an area where the climate change, simulated for the two periods, will have a quite significant effect on the daily wave characteristics. Consequently, the cumulative density in figure 4.13c shows a relatively large difference between the present and the future significant wave height distributions. Also, the probability density curve for the future climate, in figure 4.13d, is clearly shifted towards higher values. Moreover, the monthly average plot, in figure 4.13a, indicates a distinct increase of both the monthly average mean and 90th-percentile. The same trend is also seen for the monthly maximum values in figure 4.13b.

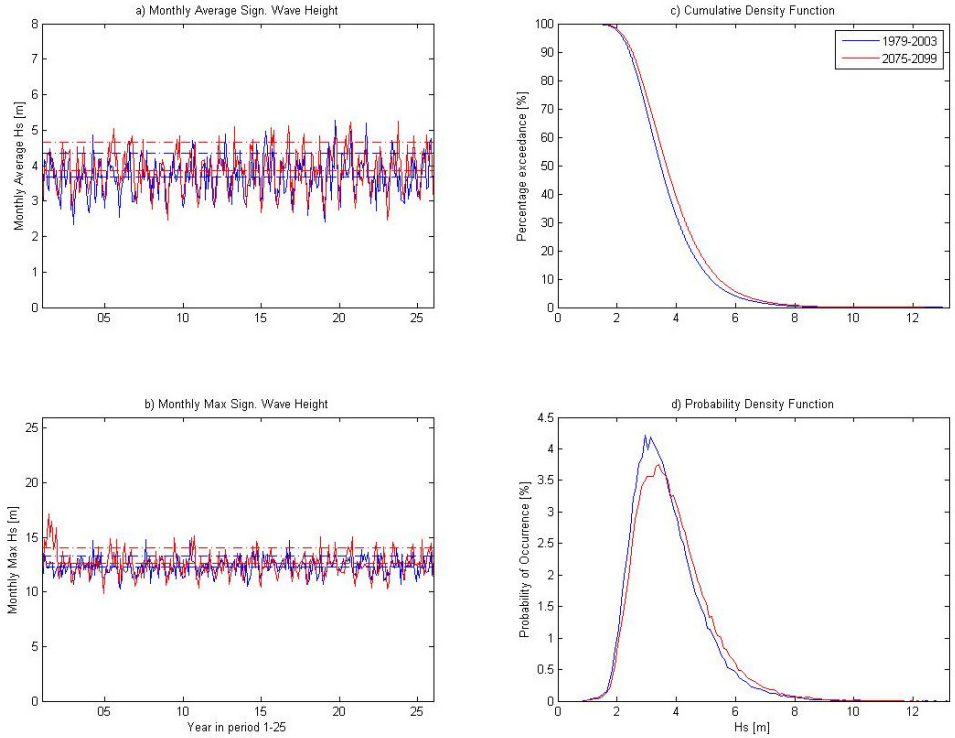

Figure 4.13 - Characteristics of the local wave height distribution of location 3. a) Series of monthly averaged significant wave height for the present and future climate simulations. b) Series of the monthly maximum significant wave height for the present and future climate simulations. In figures a-b, the mean value and 90th percentile value of the monthly data series are marked in the diagrams by dashed and dash-dotted lines respectively. c) Cumulative density function of the significant wave height for every 3rd hour. The probability of exceedance is plotted against the significant wave height. d) Empirical probability density function of the significant wave height for every 3rd hour. The probability of occurrence is plotted against the significant wave height.

In table 4.2 this change is quantified by for example, an increase of the mean significant wave height from approximately 3.7 to 3.9 m, a 5% increase. The same percental magnitude of increase is valid for all the presented percentiles, resulting in an especially important increase of the 99th percentile wave height of about 40 cm between present and future simulations.

In addition, the seasonal differences, and thus the overall spread of the distribution, are projected to increase by 8% for the 95%-spread, from a range of 4.5 to 4.8 meters. This location in thereby the one that has the largest projected differences between present and future climates.

Point 4 – South-East of Japan, Western Pacific Ocean

The fourth point is chosen because of its location in an area affected by tropical storms. The singularity of the wave climate at this site is most clearly visualized, in the boxplot in figure 4.10, where the fairly modest mean wave height together with the long upper tail of individual very large values can be seen. In figure 4.14c and d below, however, only the range of waves up to a magnitude of 10 m is shown in order to achieve a better illustration of the main part of the distribution and the change between the periods.

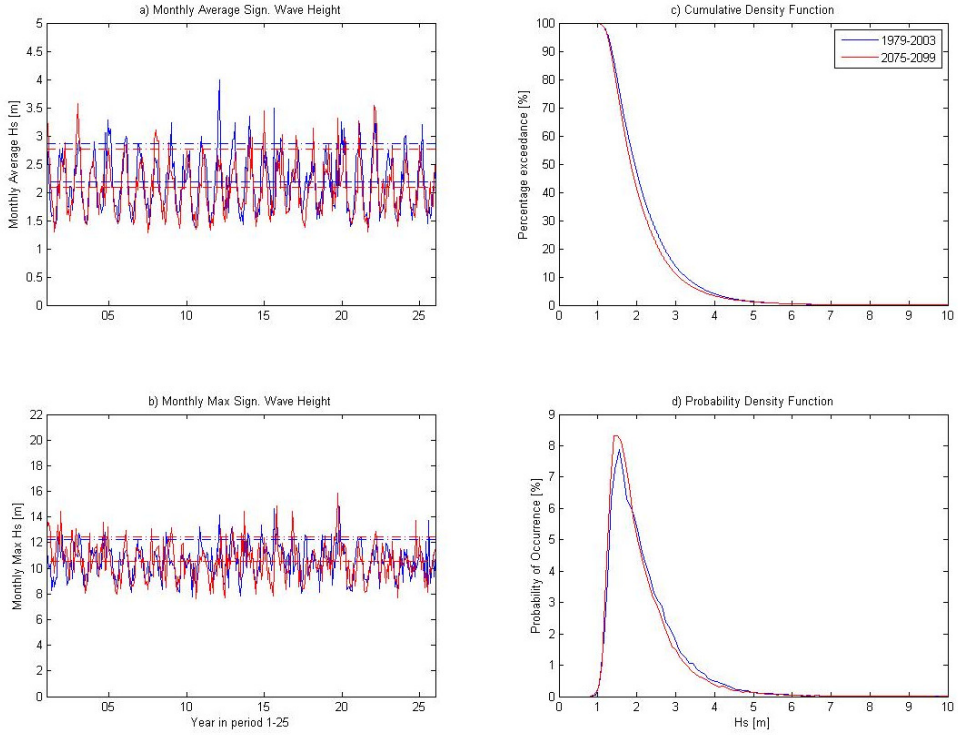

Figure 4.14 - Characteristics of the local wave height distribution of location 4. a) Series of monthly averaged significant wave height for the present and future climate simulations. b) Series of the monthly maximum significant wave height for the present and future climate simulations. In figures a-b, the mean value and 90th percentile value of the monthly data series are marked in the diagrams by dashed and dash-dotted lines respectively. c) Cumulative density function of the significant wave height for every 3rd hour. The probability of exceedance is plotted against the significant wave height. d) Empirical probability density function of the significant wave height for every 3rd hour. The probability of occurrence is plotted against the significant wave height.

The overall change from present to future climate, for this location, is negative. For the 50th to 90th percentiles the decrease is of the order 5.5%, corresponding to, an approximately reduction of 10-20 cm. For the uppermost percentile, the 99th, however, the decrease is significantly smaller, only -1.6% and less than 10 cm. This may be an indication of the different processes behind the daily wave climate and the extreme wave climate at this point. Further analysis of maximum values is presented in section 4.2.1.
Interestingly, the distribution spread for the future period at this location, is also projected to decrease quite significantly, namely by 8-9% for the quartile deviation and 80% ranges. However, the projected narrowing of the distribution is relatively much smaller, when including the outer parts of the distribution, and the 95%-spread is decreased by a mere 4.4% corresponding to 14 cm. In figure 4.14b, the mean value of the monthly maximum data set remain almost constant over the two periods.

Point 5 – Gulf of Alaska, NOAA buoy 46001
Point five is located in the Gulf of Alaska in the North Pacific Ocean, and in proximity to the NOAA buoy number 46001, which is used in the model evaluation analysis presented in section 3.1. According to the global analysis performed, this area shows only limited differences between the simulated periods 1979-2003 and 2075-2099, when comparing annual averaged data. However, the seasonal analysis showed larger discrepancies.

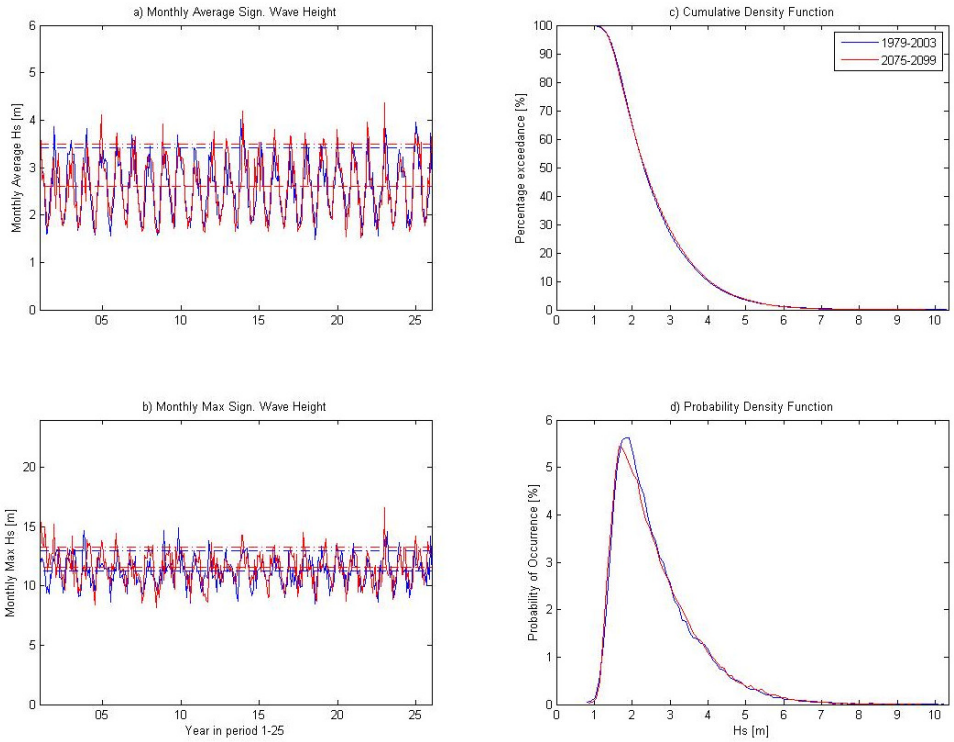

Figure 4.15 - Characteristics of the local wave height distribution of location 5. a) Series of monthly averaged significant wave height for the present and future climate simulations. b) Series of the monthly maximum significant wave height for the present and future climate simulations. In figures a-b, the mean value and 90th percentile value of the monthly data series are marked in the diagrams by dashed and dash-dotted lines respectively. c) Cumulative density function of the significant wave height for every 3rd hour. The probability of exceedance is plotted against the significant wave height. d) Empirical probability density function of the significant wave height for every 3rd hour. The probability of occurrence is plotted against the significant wave height.

As expected, based on these prior results, the cumulative density as well as the probability density in figure 4.15, shows two distributions of significant wave height of very similar appearance. The mean wave height remains constant at 2.6 m for both periods and no large alteration are noted for the other values presented in table 4.2 either.

On the contrary, the spread of the distribution increases somewhat from present to future wave climate, especially so for the quartile deviation range which increases by 6%. The overall appearance for the daily wave climate is however quite consistent for both periods.

Point 6 – Hawaii, Central Pacific Ocean, NOAA buoy 51003

The second point, chosen at the location of a NOAA buoy (number 51003), is found in the Pacific Ocean close to Hawaii. At latitude 19°N, this location if fairly close to the equatorial region and the wave climate is expected to show only minor seasonal variations, something that is verified by the plot of monthly average values, in figure 4.16a. The 95%-spread for the significant wave height distribution at this point, is just less than 2 m (table 4.3).

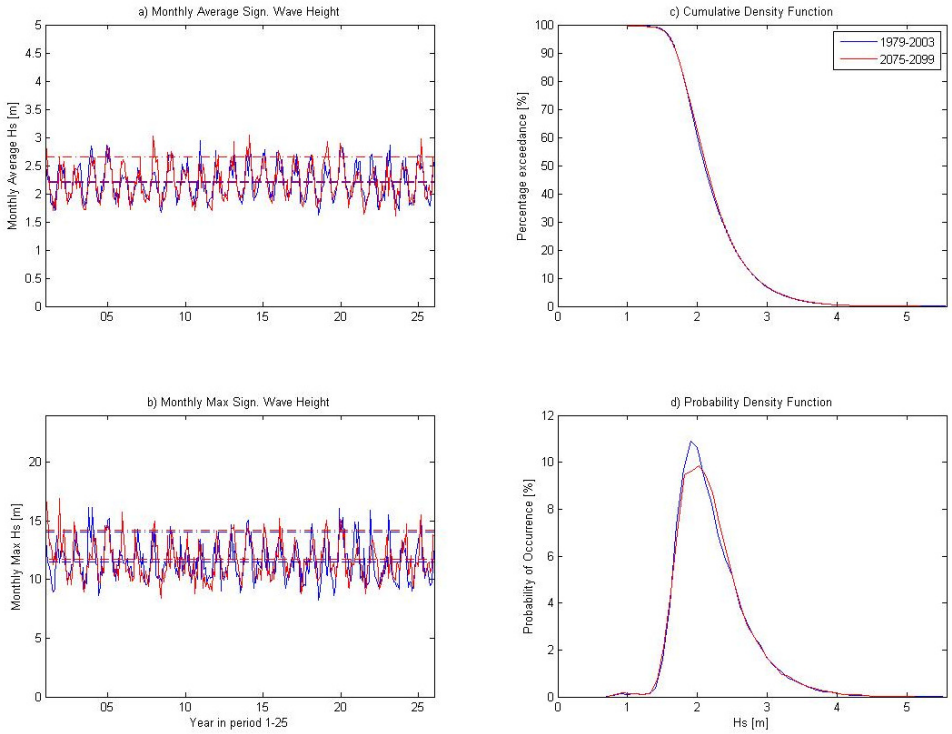

Figure 4.16 - Characteristics of the local wave height distribution of location 6. a) Series of monthly averaged significant wave height for the present and future climate simulations. b) Series of the monthly maximum significant wave height for the present and future climate simulations. In figures a-b, the mean value and 90th percentile value of the monthly data series are marked in the diagrams by dashed and dash-dotted lines respectively. c) Cumulative density function of the significant wave height for every 3rd hour. The probability of exceedance is plotted against the significant wave height. d) Empirical probability density function of the significant wave height for every 3rd hour. The probability of occurrence is plotted against the significant wave height.

Also, in the resemblance of *location 1* in on the equator in the Indian Ocean, the differences between the two periods appear to be small which can be seen in figure 4.16 where both the cumulative and probability density are similar for both periods. A slight discrepancy can be observed in the probability density for values around the distribution median value of approximately 2.10 m, where values for the future climate is larger than for the present. The median value increases only slightly however, by 1.2% while all other parameters stated in table 4.2 remain close to unaffected.

Point 7 – South Pacific Ocean

The seventh location to be analyzed is situated in the central Southern Pacific Ocean (latitude 30^{o}S) and is meant to represent characteristics of a typical mid-latitude region. The mean significant wave height is approximately 2.5 m for both periods. The changes of wave characteristics, presented in table 4.2, are negligible for this region, which is also illustrated by the appearance of the cumulative and probability densities in Figure 4.17c and d, respectively. Generally, only a marginal decrease of values at the upper end of the distribution can be seen with a decrease of 2.1% (10 cm) for the 99th percentile.

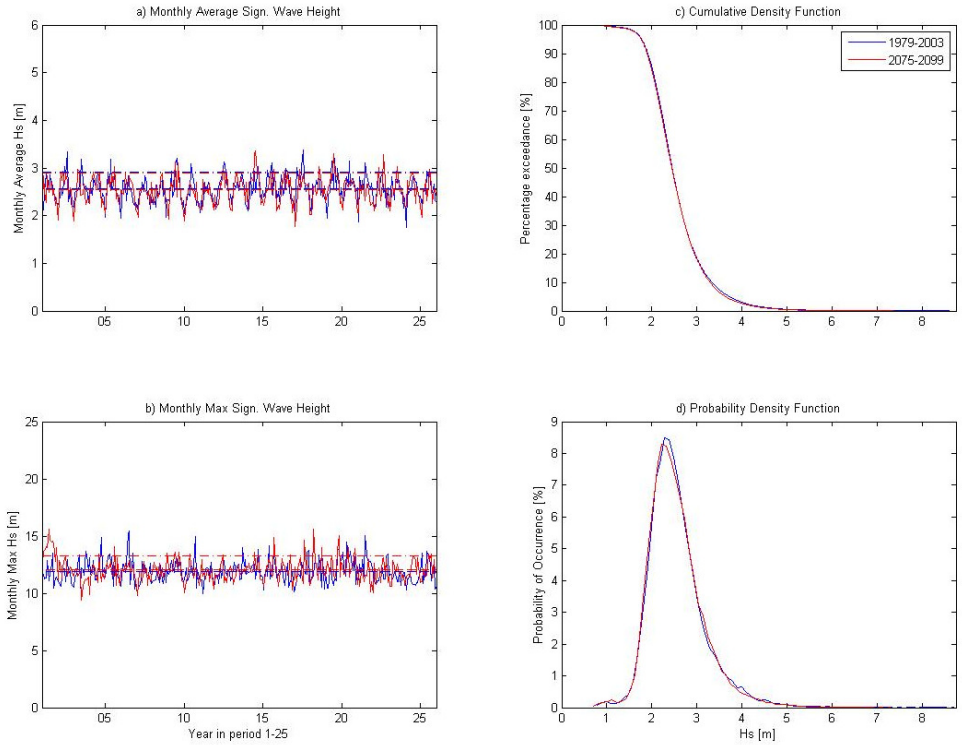

Figure 4.17- Characteristics of the local wave height distribution of location 7 a) Series of monthly averaged significant wave height for the present and future climate simulations. b) Series of the monthly maximum significant wave height for the present and future climate simulations. In figures a-b, the mean value and 90th percentile value of the monthly data series are marked in the diagrams by dashed and dash-dotted lines respectively. c) Cumulative density function of the significant wave height for every 3rd hour. The probability of exceedance is plotted against the significant wave height. d) Empirical probability density function of the significant wave height for every 3rd hour. The probability of occurrence is plotted against the significant wave height.

The seasonal variance of the significant wave height is shown in figure 4.17a. The 95%-spread of the wave height distribution is approximately 2.5 m for the present climate but is somewhat decreased, -3%, for the furure period to closer to 2.4 m.

Point 8 – Eastern South Pacific Ocean

Location eight is located in the eastern part of the Southern Pacific Ocean and is chosen because the global analysis indicated that this area experienced larger differences for the two modeled periods than surrounding mid-latitude regions.

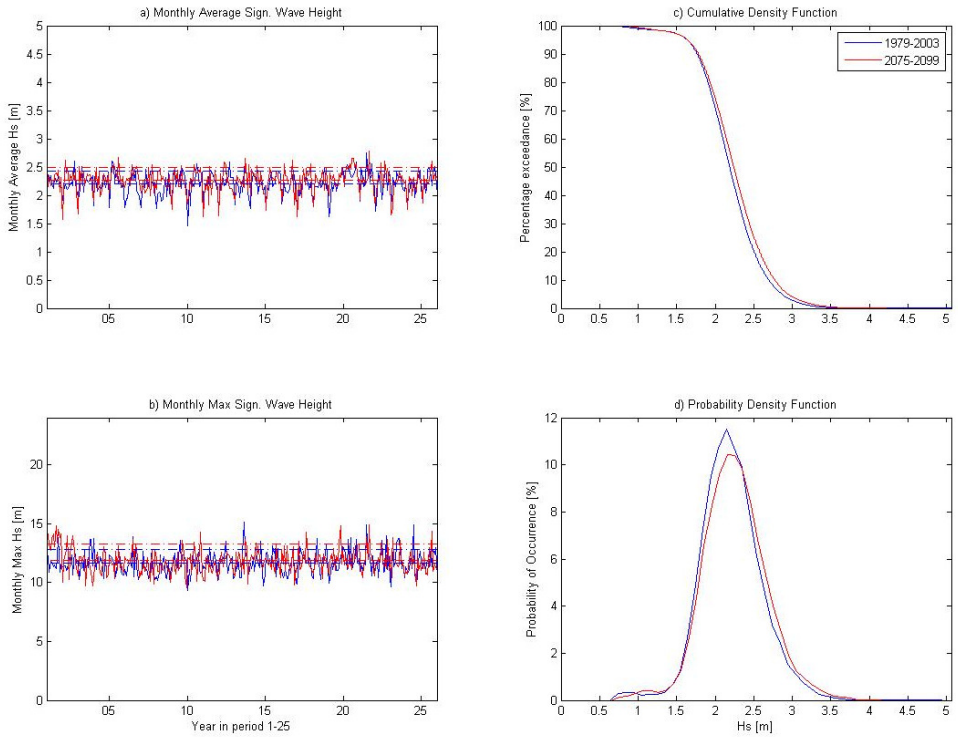

Figure 4.18 - Characteristics of the local wave height distribution of location 8. a) Series of monthly averaged significant wave height for the present and future climate simulations. b) Series of the monthly maximum significant wave height for the present and future climate simulations. In figures a-b, the mean value and 90th percentile value of the monthly data series are marked in the diagrams by dashed and dash-dotted lines respectively. c) Cumulative density function of the significant wave height for every 3rd hour. The probability of exceedance is plotted against the significant wave height. d) Empirical probability density function of the significant wave height for every 3rd hour. The probability of occurrence is plotted against the significant wave height.

The cumulative density in figure 4.18c and the probability density in figure 4.18d, clearly indicate a general increase of the significant wave height from present to future climate. The probability function shows a notable shift of the wave height distribution towards larger values. The mean wave height is increased by just over 2%, and the upper percentile values (90th and 99th) are augmented by 3-4%, corresponding to 8-13 cm. Also the monthly averages appear to be larger for the period 2075-2099.

The projections also show that the area will experience larger seasonal changes in the future, although the range of wave heights remains quite small, see table 4.3. The 95%-spread increases by 6% which, however, only corresponds to approximately 10 cm difference.

Point 9 – North Atlantic Ocean

The ninth location of this analysis is located in the northern Atlantic Ocean in an area which, according to the global analysis in section 4.1.2 and 4.1.3, experiences large seasonal variations and is also predicted to show a general decrease of significant wave height from the present to the future simulation.

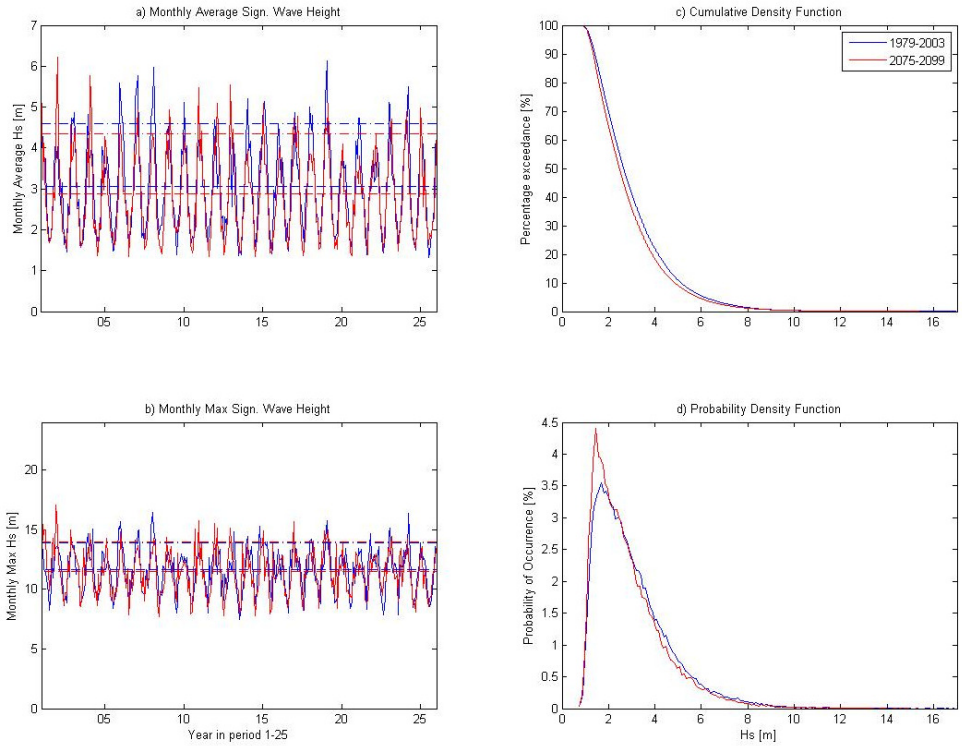

Figure 4.19 - Characteristics of the local wave height distribution of location 9. a) Series of monthly averaged significant wave height for the present and future climate simulations. b) Series of the monthly maximum significant wave height for the present and future climate simulations. In figures a-b, the mean value and 90th percentile value of the monthly data series are marked in the diagrams by dashed and dash-dotted lines respectively. c) Cumulative density function of the significant wave height for every 3rd hour. The probability of exceedance is plotted against the significant wave height. d) Empirical probability density function of the significant wave height for every 3rd hour. The probability of occurrence is plotted against the significant wave height.

The large-scale seasonal variation at this location is made very clear in figure 4.19a, showing the monthly averaged significant wave height. The 95%-spread of the wave height distribution is appreciated to be approximately 6 m, making it the largest range in this analysis. The mean and 90^{th} percentile notations in the monthly average plot, figure 4.19a also indicate that future wave height values are significantly smaller than those of the present climate. The same development is seen in the monthly maximum value series presented in figure 4.19b, where the mean value is slightly decrease. This makes this point of the few locations where the monthly maximum wave heights are not increasing.
The cumulative distribution, in figure 4.19c confirms this by showing a generally lower probability of exceedance for the period 2075-2099 than for the present climate. In addition the probability density in figure 4.19d shows a very clear peak of wave height values around 2 m. This peak is shifted somewhat towards smaller values compared to the present wave record, but most importantly the wave height distribution seems to narrow and focus around a lower average.
From table 4.2, it is found that the largest percental decrease indeed occurs in the lower wave height region of the distribution. The mean significant wave height is reduced by 6%, corresponding to 18 cm, while the value of the 99^{th} percentile is lessened by 2.2% and approximately 20 cm. The spread of the wave height distribution is also considerably reduced confirming the narrowing of the probability density function. All range measures in table 4.3, are reduced by 5-6%.

Point 10 – Southern Atlantic Ocean
The final location of the analysis is situated in the Southern Atlantic Ocean in the mid-latitude region (30^{o}S). At this point, similarly to point 9 in the northern part of the Atlantic Ocean, the general tendency is that wave height values decrease from the present climate simulation to the future.

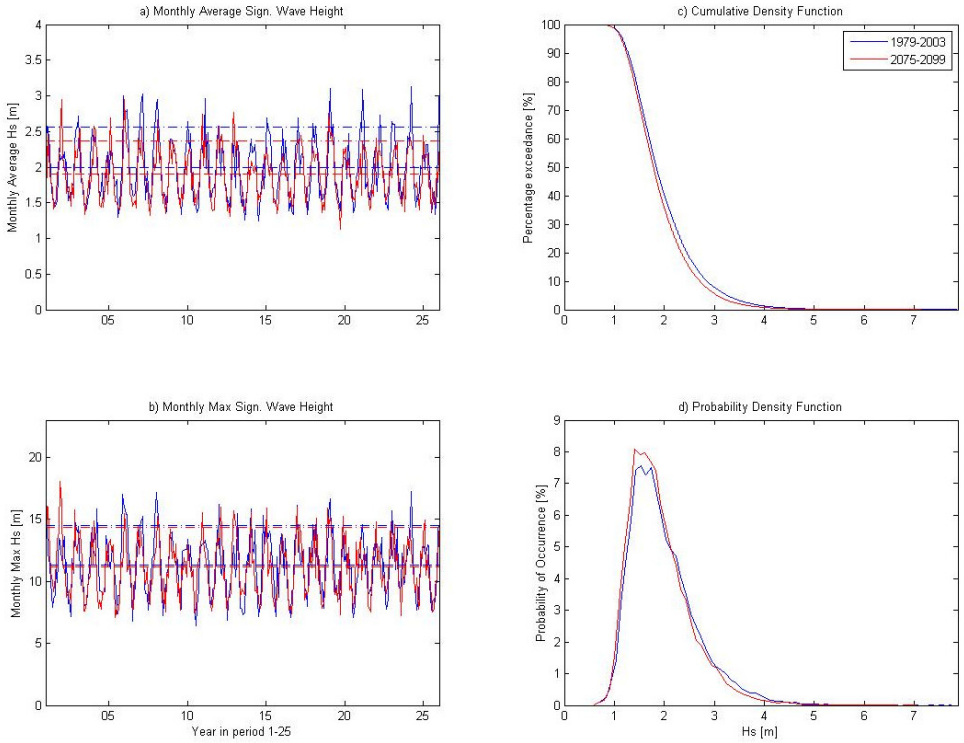

Figure 4.20 - Characteristics of the local wave height distribution of location 10. a) Series of monthly averaged significant wave height for the present and future climate simulations. b) Series of the monthly maximum significant wave height for the present and future climate simulations. In figures a-b, the mean value and 90th percentile value of the monthly data series are marked in the diagrams by dashed and dash-dotted lines respectively. c) Cumulative density function of the significant wave height for every 3rd hour. The probability of exceedance is plotted against the significant wave height. d) Empirical probability density function of the significant wave height for every 3rd hour. The probability of occurrence is plotted against the significant wave height.

All percentile values, presented in table 4.2, are decreased with approximately 3% for the lower half of the distribution and up to almost 7% for the upper region. This development is clearly illustrated by both the cumulative and probability densities in figure 4.20. The mean value for the distribution changes accordingly, from approximatly 2.0 m to 1.9 m and the uppermost value, the 99th percentile, decreases from 4.2 m to 3.9 m. For this point as well, the monthly maxima plotted in figure 4.20b, is somewhat decreased in the future simulation.

Seasonal variations are not at all as large as for in the northern Atlantic Ocean, with a 95%-spread value of approcimately 2.4 m. However the same phenomena as for location 9, of a notably reduced range of wave height values, is seen and the reduction is as large as 10% for the 95%-spread, corresponding to 25 cm.

Table 4.2 – Summary of the mean and percentile values of significant wave height, for locations 1-10. The values for the two periods are presented as well as the percental difference from the present climate simulation to the future simulation.

	Mean			*Percentiles*: 25th			50th (median)			75th			90th			99th		
Point	1	2	Change	1	2	Change	1	2	Change	1	2	Change	1	2	Change	1	2	Change
1	1.76	1.75	-0.4%	1.48	1.49	0.5%	1.73	1.73	-0.2%	2.01	2.00	-0.3%	2.25	2.24	-0.7%	2.72	2.66	-2.4%
2	2.80	2.72	-2.9%	2.08	2.04	-1.8%	2.58	2.52	-2.4%	3.30	3.19	-3.1%	4.17	3.96	-4.9%	6.12	5.91	-3.3%
3	3.67	3.87	+5.3%	2.86	2.99	+4.5%	3.48	3.67	+5.5%	4.27	4.52	+5.6%	5.18	5.46	+5.5%	7.34	7.73	+5.4%
4	2.18	2.09	-4.3%	1.57	1.52	-3.2%	1.95	1.85	-5.3%	2.54	2.40	-5.6%	3.28	3.09	-5.7%	5.26	5.18	-1.6%
5	2.59	2.60	+0.5%	1.83	1.81	-1.1%	2.31	2.33	+0.8%	3.08	3.14	+1.9%	4.03	4.06	+0.9%	6.17	6.07	-1.6%
6	2.20	2.21	+0.4%	1.86	1.87	+0.3%	2.10	2.13	+1.2%	2.44	2.45	+0.2%	2.85	2.85	+0.2%	3.76	3.78	+0.5%
7	2.56	2.54	-0.7%	2.15	1.70	-0.6%	2.45	2.44	-0.3%	2.84	2.83	-0.1%	3.34	3.30	-1.4%	4.64	4.54	-2.1%
8	2.21	2.26	+2.3%	1.96	1.99	+1.7%	2.19	2.24	+2.4%	2.44	2.51	+2.8%	2.70	2.78	+3.0%	3.22	3.35	+3.9%
9	3.04	2.86	-6.0%	1.85	1.72	-7.3%	2.66	2.48	-6.8%	3.80	3.57	-6.2%	5.15	4.88	-5.2%	8.44	8.25	-2.2%
10	1.98	1.90	-4.0%	1.50	1.46	-2.8%	1.84	1.79	-3.0%	2.32	2.22	-4.3%	2.86	2.72	-5.0%	4.16	3.87	-6.8%

Table 4.3 - Summary of the range measurements for the significant wave height distribution, for locations 1-10. The values of the quartile deviation and the 80% and 95%-ranges for the two periods are presented as well as the percental difference from the present climate simulation to the future simulation.

	Spread			Spread			Spread		
Point	25th – 75th percentile			10th – 90th percentile			2.5th – 97.5th percentile		
	1	2	Change	1	2	Change	1	2	Change
1	0.53	0.51	-2.4%	0.93	0.93	+0.2%	1.43	1.41	-3.5%
2	1.22	1.16	-5.3%	2.42	2.24	-7.3%	3.89	3.73	-5.2%
3	1.42	1.53	+7.9%	2.75	2.94	+7.0%	4.46	4.74	+7.9%
4	0.97	0.88	-9.5%	1.91	1.76	-8.3%	3.20	3.07	-4.4%
5	1.25	1.33	+6.1%	2.48	2.54	+2.3%	4.01	4.04	+1.1%
6	0.58	0.58	-0.2%	1.14	1.15	+0.6%	1.86	1.89	+1.1%
7	0.69	0.70	+1.7%	1.43	1.40	-2.1%	2.46	2.40	-2.8%
8	0.48	0.51	+7.0%	0.93	0.99	+6.5%	1.57	1.67	+6.0%
9	1.95	1.85	-5.2%	3.73	3.53	-5.4%	6.09	5.76	-5.7%
10	0.82	0.76	-7.3%	1.58	1.47	-6.9%	2.58	2.34	-9.9%

4.2.1 Analysis of extreme values based on the annual-maxima approach

The processes behind the development of everyday wave climate, which has been evaluated in section 4.2, differ significantly from the processes governing the characteristics and development of highest possible waves at a certain location. Extreme waves usually fall outside the range of the wave heights which are covered by a normal data set and therefore extrapolation is needed, in order to extend a distribution to higher values.

In order to give an indication of the development of extreme wave heights between present and future climate simulations an extreme value analysis is performed for the wave records at the ten chosen locations, defined above. For the extreme analysis the maximum value from every year of the two climate periods are chosen, thus resulting in two series of 25 values each. These data series are then to be fitted to the *Generalized Extreme Value Distribution*, as explained in section 3.3.

By choosing the annual-maxima approach for the analysis, the extreme value theory condition of independent values is accomplished. However, the data series that remain is essentially shortened which might affect the outcome of the analysis. According to the WMO (1998), the annual-maxima approach might be a realistic option for an analysis of data set of more than five years.

Since the series of annual-maxima originates in a wave record of significant wave height, these parent distributions are likely to be closely related to either the Weibull or the log-normal distribution. From this follows that the most plausible fit for an extreme value distribution is to the Gumbel shape.

The Gumbel distribution is basically the GEV distribution when the shape parameter, *k*, approaches zero, so to verify if the Gumbel distribution is a realistic choice for the data sets at hand, maximum likelihood estimations of the GEV parameters for shape, scale and location (k, σ and μ) are numerically calculated. If the Gumbel distribution is a good fit, the shape parameter, *k*, should be close to zero. It is found that at all the locations, the maximum likelihood estimate of the shape parameter, k, has a 99% confidence interval which overlaps zero. Maximum likelihood estimations of *k* are presented in table 4.4.

Table 4.4 – Maximum likelihood estimates of the shape parameter, k, with corresponding 99% confidence intervals, CI_k, for the generalized extreme value distribution function.

	Period 1		Period 2	
Location	k	99%-CI_k	k	99%-CI_k
1	-0.30	-0.77 - 0.17	0.05	-0.30 - 0.40
2	-0.05	-0.65 - 0.55	-0.01	-0.58 - 0.57
3	0.07	-0.34 - 0.48	-0.36	-0.73 - 0.01
4	0.54	-0.05 - 1.13	0.34	-0.14 - 0.81
5	-0.37	-0.86 - 0.11	-0.21	-0.64 - 0.22
6	-0.24	-0.73 - 0.25	-0.56	-1.29 - 0.17
7	-0.25	-1.02 - 0.51	-0.28	-0.74 - 0.19
8	0.25	-0.23 - 0.73	-0.27	-0.58 - 0.03
9	-0.18	-0.64 - 0.27	-0.27	-0.71 - 0.18
10	-0.13	-0.38 - 0.12	0.06	-0.32 - 0.43

Based on this result, the Gumbel distribution appears to be a reasonable fit for the annual-maxima data sets and is consequently chosen for the estimation of return values. In figure 4.21, the fitted distributions are displayed for the relationship between return period in years and the corresponding return value of annual-maximum wave height, $H_{s,am}$.

The overall correspondence between the data sets and the Gumbel distribution appear to be quite good. However a few deviating large wave height values, at points 6, 7 and 10 are slightly troublesome. It is possible that the distributions at these points would gain a better fit to the annual maxima extra weight was attributed to the largest values of the data set. However, since the deviations mainly indicate a reduction of the return values this is left for future investigation at this point.

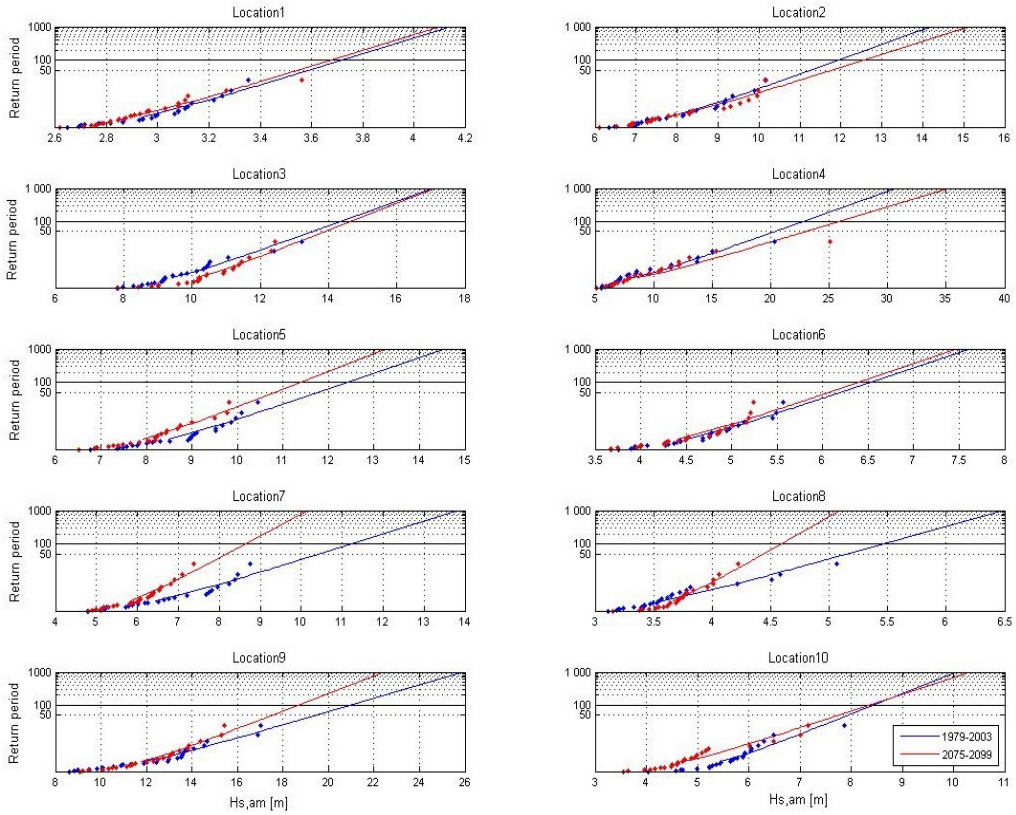

Figure 4.21- Estimations of the Return Period-Return Value relationship for locations 1-10. The relationships are based on the annual-maxima from the two data sets for present and future climate, which have been fitted to the Gumble extreme value distribution by mean of maximum likelihood estimation. On the vertical axis, return periods up to 1000 years are plotted, against the corresponding value of extreme wave height on the vertical axis.

Although figure 4.21 presents values for return periods as high as 1000 years, these upper values should be looked upon with caution, since extrapolation far into the future brings increasing uncertainty to the estimations. The values corresponding to the 50 and 100-year return periods are presented in table 4.5 together with the difference between the present and future climate simulations.

Table 4.5 – Estimation of return values of wave height for return periods of 50 and 100 years for the present and future climate simulations.

	Return values for 50-year return period			Return values for 100-year return period		
Location	1979-2003	2079-2099	Difference	1979-2003	2079-2099	Difference
1	3.6	3.5	-3%	3.7	3.7	-
2	11.3	11.8	+4%	11.9	12.6	+6%
3	13.5	13.9	+3	14.4	14.7	+2%
4	20.4	23.0	+13%	22.8	25.9	+14%
5	11.8	10.8	-9%	12.4	11.4	-8%
6	6.2	6.1	-2%	6.5	6.4	-2%
7	10.4	8.2	-21%	11.2	8.6	-23%
8	5.2	4.4	-15%	5.5	4.6	-16%
9	19.5	17.5	-10%	21.0	18.7	-11%
10	7.9	7.8	-1%	8.4	8.4	-

From figure 4.21 and the values in table 4.5 it is seen that the development of the extreme wave climate also varies significantly based on location. For points 1, 2, 3, 6 and 10, the return values are almost the same for both present and future climate showing differences of only a few percent's variation for values corresponding to a 50-year return period.

Both points situated in the southern Pacific Ocean, 7 and 8, show large reductions of the return values of about 15-20%. The same trend is shown for the two locations in the Northern Hemisphere, points 5 in the Gulf of Alaska, and point 9 in the North Atlantic Ocean. The decrease of the future estimations of the return values is in the order of about 10%. The percental reductions at these locations correspond to return values that are decreased by 1-2 meters which is quite an important difference which might be noticeable to marine activities in those regions.

The only location that shows a large increase of the return values is point 4, placed in a region affected by tropical storms. Since the extreme value theory is based on the condition that the evaluated data set is equally distributed the annual-maxima approach, which is used here might not be particularly suitable approach for a location such as this. Again, the differences of the physical processes behind regular large waves and waves that originate from extreme events such as tropical storms should be treated separately. The result, for location 4, as shown in figure 4.21 might well describe the general wave climate in this region, but to get reliable estimates of the extreme conditions further analysis should be conducted for example focusing on individual storms.

4.3 Summary

To summarise the results presented in section 4, firstly the strong latitude dependence of both wave and wind characteristics must be acknowledged. The highest waves, as well as the largest seasonal differences are found in the mid to high latitude regions of both hemispheres. In addition, the largest simulated changes from present to future climate, 1979-2003 to 2075-2099, are seen in these same areas.

The largest increases from the present to future wave simulations are located in the southern parts of the Indian, Atlantic and to some extent the Pacific Oceans, with the area south of Australia and New Zeeland seemingly being the most affected region. Based on the local climate analysis in section 4.2, for point 3 which is situated in this area, the overall increase is estimated to be in the order of 5% for the full range of the significant wave height distribution. Also, a quite significant increase of the seasonal variation range is recognized at this location.

In contrast, the most substantial decreases of the significant wave height between present and future climate simulations is found in the North Atlantic Ocean where the period averaged significant wave height show widespread reductions of over 5%. The same phenomenon is represented in the wave distributions of the local wave climate analysis at location 9, in section 4.2, where both the overall magnitude of significant wave height and the corresponding annual wave height range are decreased for the future wave simulation.

In the western part of the North Pacific Ocean, another area experiencing a decreasing averaged wave climate is worth acknowledging. The reduction in this area is of lesser magnitude than that of the North Atlantic Ocean, approximately in the order of 2.5% up to local reductions of almost 5%. However, the affected area is quite large and interestingly positioned in an area known to be frequented by extreme events such as tropical cyclones. While the analysis in sections 4.1 and 4.2 give no information about changes in the frequency or magnitude of extreme events, the reduction in this area is nonetheless interesting, when put in contrast to the indication that the future wave climate in this area outside Japan will in the future host more larger waves than the present climate.

Seen globally, the overall change from the present to the future simulated wave climate is strongly correlated to spatial location, and thus shows both negative and positive trends on a regional scale. For the largest spatial extent of the world oceans, however, the net change of significant wave height for the future climate simulation appear to have very limited or slightly negative effect on the wave climate, exceptions being the high-latitude regions discussed above.

5 Conclusions

The study presented in this report show projected future changes in global wave climate fields derived from the wind field output of the JMA/MRI-AGCM3.2 model. The wave fields are numerically modelled by the WAM model with a resolution of 1 degree. The aim of the study is to give an overview of impending changes in wave climate from present to future under the effects of climate change.

Focusing on wave fields during normal climate conditions, the modelled results are thought to give a good overall estimation to how the wave climate is affected by the projected climate change. On the other hand, more in depth research of regional climate variations would be needed in order to give a realistic analysis of the future development of extreme events. Such research would also require for the simulations to be run with a higher resolution since processes behind extreme events such as tropical cyclones are governed by many small-scale phenomena which are difficult to evaluate with a large-scale model.

The evolution of the average wave climate from present to future climate is nevertheless, well-represented by the performed simulations, and has been evaluated both on a global scale as well as for some chosen locations spread over the world. The initial evaluation of the model performance, through the comparison of the modelled wave and wind data sets to observed buoy measurements, indicates that there are notable differences between the modelled and observed local wave and wind conditions. While the mean significant wave height of the modelled wave records correspond very well to observed values, the average wind speed is overestimated by 13.5%.

This result is somewhat disturbing since the accuracy of the input wind fields into the WAM model is directly connected to the results of the wave climate simulations, and errors in the wind fields can have cumulative effect on the accuracy of the simulated wave climate. However, it is important to note that the comparison of the buoy measurements to modelled values with a resolution of 1 degree, is not without complications in itself, and it is possible that the indicated errors are less extensive than they seem. For this study, where the main focus lies on the comparison between two different climate periods the deviation from the observed values are not thought to cause extensive problems.

The results of the analysis of the global wave climate give a very clear idea of where, and by how much the wave climate is plausible to change based on the projected evolution of the climate. There is no unanimous trend of increasing or decreasing wave height since the evolution of the wave climate is very strongly related to location. The regions of furthermost interest in the assessment of future changes of wave climate are found to be the mid- to high latitudes, with significant increases, in the order of 5%, in the Southern Hemisphere and local regions of the northern Pacific Ocean, and decreases of the same magnitude in especially the North Atlantic Ocean.

Large parts of the world appear to go quite unaffected through the projected climate change. It is however important to remember that this analysis is mostly

limited to the average and everyday wave climate, and thus does not account for possible changes of events going outside the range of normal climate conditions. One region where this is especially important to keep in mind is the western part of the North Pacific Ocean, off the coast of Japan, which shows an overall decrease in averaged significant wave height but a large increase of wave height in the assessment of the annual maxima.

When building coastal and off-shore structures, the design conditions are usually based on extreme values of wave height, typically with return period of 100 years or more. The everyday wave climate also put strain on these structures though in a less immediate way. In some regions, such as the areas south of Australia and New Zeeland, where the significant wave heights are projected to increase significantly for the future climate there would in the future, be reasonable to re-evaluate the fatigue effects induced on coastal and marine structures, from the increasing and persistent wave climate.

To continue this research, a higher resolution simulation of the wave climate is recommended in order to give better detail for the assessment of extreme events and tropical cyclones. It would be interesting to compare the future effects on the daily wave climate, analysed here, and the evolution of the extremes for the corresponding areas. The newly developed AGCM model used in this study can be run for large scale, even global simulations, for very high resolutions making it a fine tool for future wave climate analysis.

6 Acknowledgement

I would like to take this opportunity to express my warmest appreciation and gratitude towards Kyushu University and all the friendly and helpful people that I have met here during my stay in Fukuoka.

I would especially like to thank my supervisor Professor Noriaki Hashimoto of the Department of Maritime Engineering, at Kyushu University, for his friendship and guidance through the complex world of ocean waves. Also, my deep gratitude goes out to Mr Zikra and Mr Kodama, of the Coastal and Ocean Engineering Laboratory, who both have aided me and provided much useful input to my research.
I would also like to thank Professor Magnus Larson at the Department of Water Resources Engineering at Lund University, who although half a world away, has continuously helped me through useful feedback and ideas.

Lastly, I am extremely thankful to all the members of the Coastal and Ocean Engineering Laboratory for their warm and welcoming friendship as well as all the support I have received during my acclimatisation to the sometime confusing life in Japan. My stay here wouldn't have been half as good without you!

Thank you!

Johanna

7 Bibliography

ECMWF. (2011). *IFS DOCUMENTATION – Cy37r2. PART VII: ECMWF WAVE MODEL.* Reading, UK: European Centre for Medium-Range Weather Forecasts.

Holthuijsen, L. H. (2007). *Waves in Oceanic and Coastal Waters.* Cambrige, UK: Cambridge University Press.

IPCC. (2000). *IPCC Special Report. Emission Scenarios.* Cambridge, UK: Cambridge University Press.

IPCC. (2001). *Climate Change 2001: The Scientific Basis. Contribution of Working Group I to the Third Assessment Report of the Intergovernmental Panel on Climate Change.* Cambridge, UK and New York, USA: Cambridge University Press.

IPCC. (2007). *Contribution of Working Group I to the Fourth Assessment Report of the Intergovernmental Panel on Climate Change.* Cambridge, United Kingdom and New York, NY, USA: Cambridge University Press.

Janssen, P. (2004). *The Interaction of Ocean Waves and Wind.* Cambridge, UK and New York, NY, USA: Cambridge University Press.

Janssen, P. A., Günther, H., Hasselmann, S., & Zambresky, L. (1994). III.5 The WAM Model Software Package. In G. J. Komen, L. Cavaleri, M. Donelan, K. Hasselmann, S. Hasselman, & P. A. Janssen, *Dynamics and Modelling of Ocean Waves* (pp. 239-244). Cambridge: Cambridge University Press.

Kitoh, A., Ose, T., Kurihara, K., Kusunoki, S., Sugi, M., & KAKUSHIN Team-3 Modeling Group. (2009). Projection of Changes in Future Weather Extremes Using Super-High-Resolution Global and Regional Atmospheric Models in the KAKUSHIN Program: Results of Preliminary Experiments. *Hydrological Research Letters, 3*, 49-53.

Mizuta, R., Oouchi, K., Yoshimura, H., Noda, A., Katayama, K., Yukimoto, S., et al. (2006). 20-km-Mesh Global Climate Simulations Using JMA-GSM Model. *Journal of the Meteorological Society of Japan, Vol 84*, 165-185.

Mizuta, R., Yoshimura, H., Murakami, H., Matsueda, M., Endo, H., Ose, T., et al. (2011). Climate simulations using MRI-AGCM3.2 with 20-km grid. *Journal of the Meteorological Society of Japan*, accepted Nov. 2, 2011 (not yet published).

Mori, N., Yasuda, T., Mase, H., Tom, T., & Oku, Y. (2010). Projection of Extreme Wave Climate Change under Global Warming. *Hydrological Research Letters, 4*, 15-19.

Murakami, H., Mizuta, R., & Shindo, E. (2011). Future Changes in Tropical Cyclone Activity Projected by Multi-Physics and Multi-SST Ensemble Experiments Using the 60-km-mesh MRI-AGCM. *Climate Dynamics*.

Onogi, K., Tsutsui, J., Koide, H., Sakamoto, M., Kobayashi, S., Hatsushika, H., et al. (2007). The JRA-25 Reanalysis. *Journal of the Meteorological Society of Japan, Vol 85*, 369-432.

Pierson, W. J., Neumann, G., & James, R. W. (1955). *Practical methods for observing and forcasting ocean waves by means of wave spectra and statistics.* US Navy Hydrographic Office Publications.

Reeve, D. T. (2011). *The Stocastic Analysis of Ocean Waves: Vital for the Design and Safe Operation of Offshore Structures.* Lancaster, UK: University of Lancaster.

Suzuki, Y., Sato, Y., & Michihiro, Y. (2011). Global Warming Impact on Hydrologic Environment from Climate Change Projections. *International Seminar on Water Related Risk Management.* Jakarta, Indonesia: Water Resources Research Center, Disaster Prevention Research Institute, Kyoto University.

Taylor, K. E. (2001). Summarizing multiple aspects of model performance in a single diagram. *Journal of Geophysical Research, 106*, 7183-7192.

WAMDI Group. (1988). The WAM-model - A Third Generation Ocean Wave Prediction Model. *Journal of Physical Oceanography. Vol 18*, 1775-1810.

Wang, X., Zwiers, F., & Swail, V. (2004). North Atlantic Ocean Wave Climate Change Scenarios for the Twenty-first Century. *Journal of Climate, 17*, 2368-2383.

Weisse, R., & von Storch, H. (2009). *Marine Climate and Climate Change. Storms, wind waves and Storm Surges.* UK: Praxis Publishing.

WMO. (1998). *Guide to Wave Analysis and Forecasting (Second Edition).* Geneva, Switzerland: World Meteorological Organization.

Wu, J. (1982). Wind-Stress Coefficients Over Sea Surface from Breeze to Hurricane. *Journal of Geophysical Research, 87*, 9704-9706.

Vännman, K. (2002). *Matematisk Statestik.* Lund, Sweden: Studentlitteratur.

8 Appendix A

Global Visualisation of Monthly Distributions of the Period Averaged Significant Wave Height.

In figures A.1 and A.2 the spatial distributions of the global significant wave height is presented. Each graph shows the period averaged significant wave height for one month for the present (figure A.1) and future (figure A.2) climate simulations.
These distributions are used as visual aid in the process of dividing the year into suitable seasonal divisions, used in section 4.1. The aim is to gain four seasonal periods of three months each that best describe the global variations throughout the year.
From the figures it is clear that the highest wave heights occur during winter in both the Northern and Southern Hemispheres. The months that most evidently show these characteristics are December to February for the Northern Hemisphere and June to August for the Southern Hemisphere. Accordingly the year is divided into winter, December-February; spring, March-May; summer, June-August and fall season, September-November.

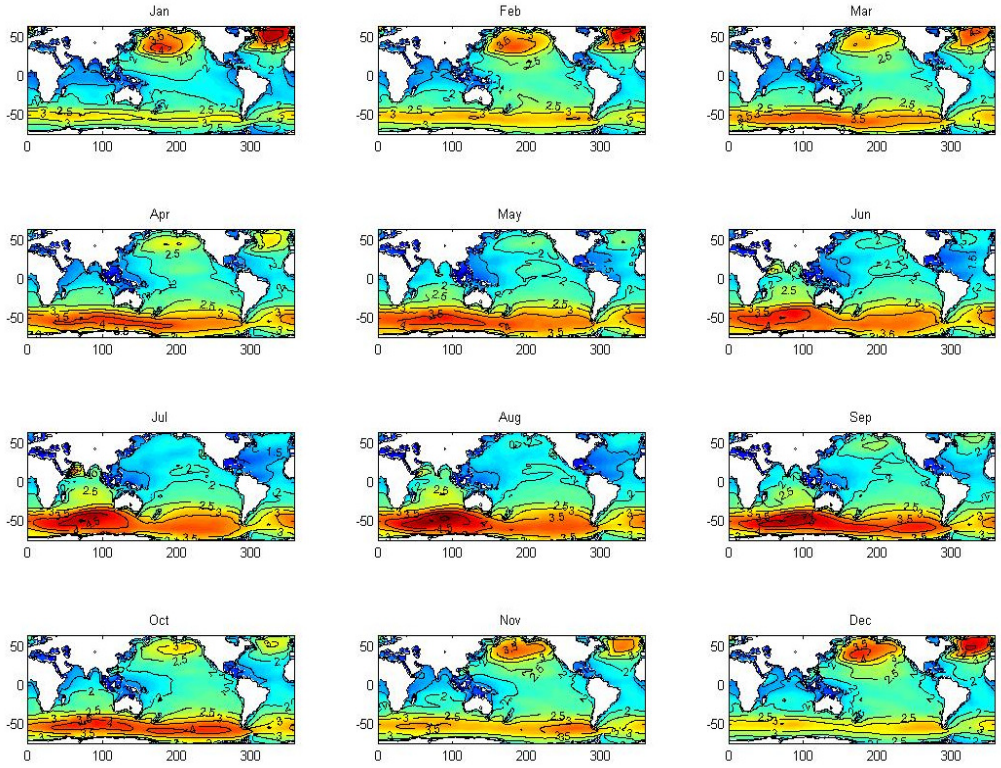

Figure A.1 – Spatial distribution of the monthly averaged significant wave height for the period 1979-2003.

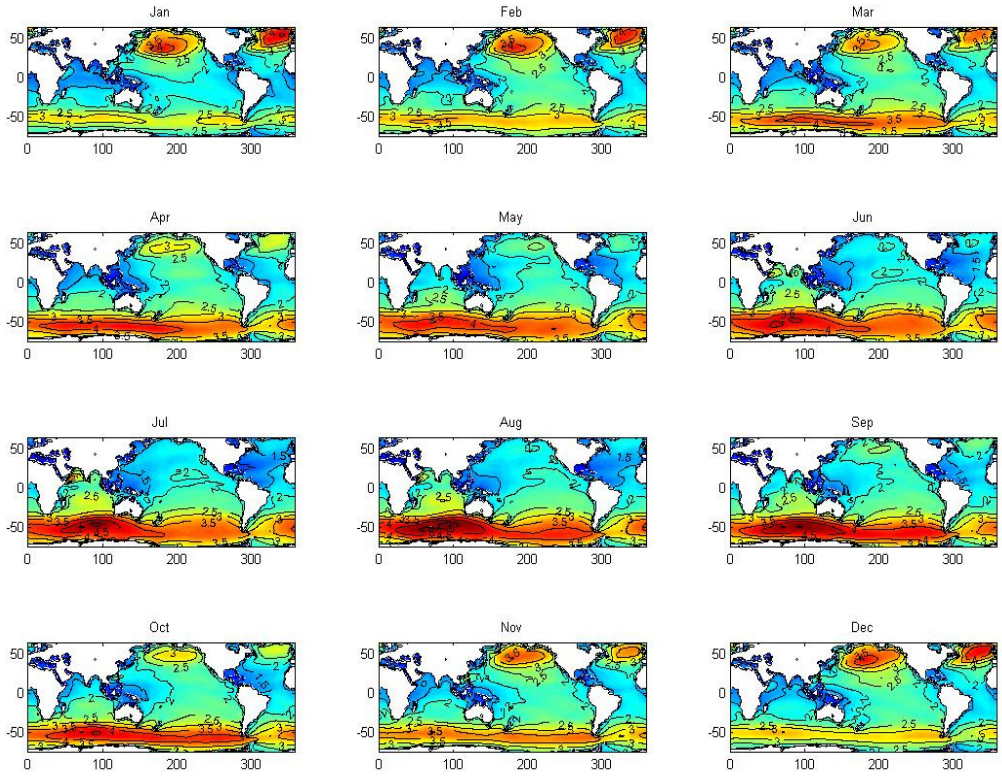

Figure A.2 - Spatial distribution of the monthly averaged significant wave height for the period 1979-2003.